Photocatalysts for CO2 Reduction and Computational Insight

Yakubu Adekunle Alli, Peter Olusakin Oladoye, Abdulmujeeb T Onawole, Hazleen Anuar, Sheriff Adewuyi, Daniel Ogunbiyi, Karine Philippot

Photocatalysts for CO_2 Reduction and Computational Insight

Yakubu Adekunle Alli[a,b,e**], Peter Olusakin Oladoye[c,*], Abdulmujeeb T. Onawole[d], Hazleen Anuar[e], Sheriff Adewuyi[f], Olutobi Daniel Ogunbiyi[c], Karine Philippot[a]

[a]Laboratoire de Chimie de Coordination du CNRS, UPR8241, Université de Toulouse, UPS, INPT, Toulouse cedex 4 F-31077, France.

[b]Department of Chemical Sciences, Faculty of Science and Computing, Ahman Pategi University, Patigi-Kpada Road, Patigi, Kwara State, Nigeria

[c]Department of Chemistry and Biochemistry, Florida International University, 11200 SW 8th St, Miami, FL, 33199, USA

[d] Department of Chemistry, King Fahd University of Petroleum and Minerals, KFUPM, Dhahran 31261, Saudi Arabia

[e] Department of Manufacturing and Materials Engineering, Kulliyyah of Engineering, International Islamic University Malaysia, Jalan Gombak, 53100 Kuala Lumpur, Malaysia

[f] Department of Chemistry, Federal University of Agriculture Abeokuta, Ogun State Abeokuta, 2240, Nigeria

[*]Corresponding author's e-mail address: poladoye@fiu.edu

[*]Corresponding author's address: Department of Chemistry and Biochemistry, Florida International University, 11200 SW 8th St, Miami, FL, 33199, USA

[**]Corresponding author's e-mail address: yakubu.alli@lcc-toulouse.fr

[**]Corresponding author's address: LCC-CNRS, Université de Toulouse, CNRS, UPS, 205 Route de Narbonne, BP44099, 31077 CEDEX 4 Toulouse, France

Abstract

Global warming is caused by excessive CO_2 production, and reducing CO_2 emissions is a viable way to counteract this. It has been extensively studied how light-driven processes, particularly photocatalytic systems, can transform solar energy into chemical energy. In the present review exercise, the mechanism of CO_2 reduction is described using calculations based on density functional theory (DFT), and comparisons are also made with regard to typical light-driven devices. Additionally, the traits of potential

materials—including metal-organic frameworks (MOFs), metal complexes, semiconductors, Z-scheme (metal complexes/semiconductors, two semiconductors, Dye-sensitized semiconductors) and organic semiconductors etc.—are described in depth to show how these traits affect the CO_2 adsorption, activation, and desorption processes. Also summarized are a number of methods for enhancing the selectivity and efficiency of catalytic reactions. Lastly, the challenges and future outlook of light-driven reactions for CO_2 reduction are presented.

Keywords: Photocatalysts; CO_2 reduction; Semiconductors; Z-schemes; MOFs

Table of contents

1. Introduction

The global increase in population has a correspondingly warranted an increase in the usage of fossil fuels for the existence of mankind. This is a result of the need to use some technologies powered and/or driven via the use of various forms of fossil fuels, with associated emission of CO_2 into the atmosphere at a yearly estimated emission rate of 3.0×10^{13} kg per year [1]. Simply put, this large use of fossil fuels has only been able to satisfy the world energy demand by ~81% [2]. The temperature rises due to this huge CO_2 input into the atmosphere causing a number of harms to the global populace such

as global warming, flooding, etc. This was corroborated at the Paris Conference held by the United Nations Agreement, which highlighted that the combustion of fossil fuels, leading to the emission of CO_2 and stored in the atmosphere, could increase the global temperature of the atmosphere owing to the unequal intensity of incoming and outgoing solar energy [3]. Hence, in order to ameliorate the various health and environmental impacts, due to CO_2 emission, various reduction and/or transformation technologies have been designed by researchers.

Amongst the available technologies that have been applied to convert or reduce CO_2 are photocatalytic transformation [4,5], thermal conversion, electrocatalytic conversion [6,7], biological approach (fixation) [8,9], electrochemical transformation [10,11] and so on. In terms of efficiency, the application of catalytic or thermal transformation is limited due to the involvement of high pressure and temperature with associated or elevated process operational cost; although the two technologies have been found to be effective [12,13]. The efficiency of the electrochemical conversion of CO_2 to value-added hydrocarbon fuels is low and limits its widest application [14]. Likewise, the biological approach is impractical because of the requirements of enzyme production and the need for regeneration that are germane to the functionality of the process [15,16]. However, photocatalytic conversion has overwhelming merits when compared to others, as it primarily makes use of solar energy and photocatalyst for conversion.

Photocatalytic conversion has been described as an "artificial photosynthetic" route for the transformation of CO_2 to useful hydrocarbon and hydrogen fuels. In this vein, various previous studies have reported the use of a photocatalytic approach for the reduction and/or conversion of CO_2 [17] to methanoic acid (HCOOH) [18,19], methane (CH_4) [20,21], methanal (HCHO) [22] carbon monoxide (CO) and [23,24] and methanol (CH_3OH) [7,25]. Sequel to the applicability, effectiveness, eco-friendliness, cheapness and practicability of this method, several authors have worked on and/or reported the use of different photocatalysts to capture and reduce, by conversion of CO_2, to the above-mentioned products via "artificial photosynthetic" route. For instance, several researchers have worked on the use of metal-organic frameworks, organics, z-scheme, semiconductors, and metal complexes as photocatalysts for CO_2 conversion. In addition, a number of studies have been done in the use of computational studies to investigate the effectiveness or efficacy of photocatalysts for CO_2 conversion

in the presence of solar energy, before experimental work is done. Examples are the use of Density Functional Theory (DFT) and Artificial Intelligence (AI) tools such as Machine Learning (ML) and Deep Learning (DL). These tools are and becoming widely used and might be integrated into the conventional workflow research workflow of photocatalytic conversion of CO_2 conversion.

Recently, Sharma et al. published a review article on photocatalytic conversion or reduction of CO_2 using ZnO/carbon hybrid [26]. Wang et al. evaluated research papers published on CO_2 reduction using copper-based photocatalysts [27]. Devi et al. presented previous reports, by evaluation, on photoelectrochemical, electrochemical and photocatalytic reduction of CO_2 [28]. This article either narrow their evaluation to a single material as photocatalyst, or compare a limited number of methods. However, in this review, we reported on the usefulness, effectiveness and applicability of the computational approach in photo-catalytically reducing and/or transforming CO_2 as described in section 2 of this article. We explained briefly the fundamental mechanism of photocatalysis in section 3. Furthermore, detailed formation gathered from scattered literatures on metal complexes, metal oxides, z-scheme, S-scheme and organic as enviable photocatalysts were thoroughly evaluated and presented in sections 4, 5, 7, 8, and 9 respectively. Metal-organic frameworks (MOFs), which are porous materials for adsorption, and which also possess photocatalytic properties [29], were discussed in section 6, by evaluating their CO_2 capture capacity, CO_2 photoconversion, mechanism of CO_2 photo-reduction and the challenges of MOFs synthesis and application. Finally, the review concludes by advocating the use of theoretical (computational) studies in the conduction of experiments for photocatalytic CO_2 reduction or conversion, in order to have a prior understanding of the effectiveness of photocatalysts to be employed for the transformation process.

2. Computational studies of photocatalysts for CO_2 reduction

Computational studies have become quite popular in most recent studies involving the application of materials that have photosensitizing properties for CO_2 reduction [1–4], particularly the Density Functional Theory (DFT) method making it an indispensable tool in present-day research. This is no surprise as DFT studies complement experimental works by providing atomistic insights into how the molecules studied have photosensitizing abilities capable of reducing CO_2. DFT studies help to understand the mechanism of action or pathway of CO_2 reduction by the studied materials. This

aids the modification and development of better materials. DFT has many tools including Geometry optimization, electrostatic potential maps, TD-DFT (Time-Dependent Density Functional Theory) for UV-Visible calculated spectra, molecular orbital maps, and intrinsic reaction coordinate systems, free energy profiles which are used in studying these materials. However, these are often used for studying molecules. On the other hand, Periodic DFT can study larger systems which include the molecules on catalytic surfaces.

Geometry optimization is usually the first calculation carried out on the studied system. In the case where the studied material is made up of complexes that contain transition metals. This can be sometimes challenging as a trade-off is often made between accuracy and computational costs this is further exacerbated by the spin-state energetics [5–8]. The B3LYP functional [9] with the 6-31G(d,p) basis sets is a renowned and accurate level of theory and basis set respectively for non-metal atoms in the system whilst the TZVP (Triple Zeta Valence with Polarization) basis set is more reliable for metals even though it comes at an additional computational cost [10,11]. Geometry optimizations are often used to compare and validate the bond parameters (bond lengths and angle) to experimental crystal structures derived from Single-crystal X-ray diffraction. The molecular orbitals consist of the HOMO (Highest Occupied Molecular Orbital) and Lowest Unoccupied Molecular Orbital (LUMO) and are also used in calculating energy gaps and deducing the wavelength of the excitation energies of the studied material.

For instance, in the DFT calculations done by Zhou et al [12] on MCOF-Ti_6Cu_3, a metallic cluster catalyst deduced from the closeness of the HOMO and LUMO the cluster could be excited by infrared light (1704.16 nm) excitation energy. The HOMO-LUMO maps also help to understand the distribution of electron clouds within the studied material and the transfer of electrons during the excitation process. This can be quite useful in confirming what was observed from in situ X-ray photoelectron spectroscopy (XPS) experimental measurements. Zhou et al were able to prove with the aid of DFT that reduction occurred on the Cu cluster whilst oxidation occurred on the Ti cluster. DFT studies are also used to investigate the non-covalent interactions (NCI) in the metallization of porphyrinic photosensitizers. Yin et al [13] employed DFT to investigate the NCI between porphyrin-based hydrogen-bonded organic framework molecules and different metals (Co, Ni, Cu, Zn). Their result showed that upon

metallization of the porphyrinic material the core changes the π - π stacking interaction and consequently the NCI between interlayer adjacent porphyrin rings. This was further confirmed by the orbital overlaps when observing the HOMO-LUMO maps. Summarily, this showed that metallization bestowed the porphyrins with different catalytic activities useful for CO_2 photoreduction. Amongst the porphyrin-metallization studied, the one with cobalt showed optimal performance. However, the recent work by Torre et al [14] used DFT calculations to predict that the source of different behaviour observed in Fe^{2+} and Co^{2+} complexes is the electronic configuration of the reduced species. That is from Co^{2+} to Co^{+}, the reduction is predicted to be metal-centred leading to an observed loss in CO_2 reduction reaction (CO_2RR) activity and increased Hydrogen Evolution Reaction (HER) from a formal Co^{+} than Co^{2+}. Further reduction from Co^{+} to Co^{o} is accompanied by significant electron rearrangement to a metal-ligand coupling interaction in the form of an open shell doublet with a formal Co^{2+} center bound to a twice reduced ligand, in this case $(tpyPY2Me^{**})^{2}$. Though experimental analysis such as electrolysis and photocatalysis experiments suggest that this reduced specie is capable of reducing CO_2 to CO but not stable which leads to the formation of a nanoparticle film. When used in metal-ligand exchange coupling, the understanding of this instability caused by the open-shell doublet is due to DFT calculations. **Figure 1** shows the DFT optimized structure of the cobalt metal-ligand.

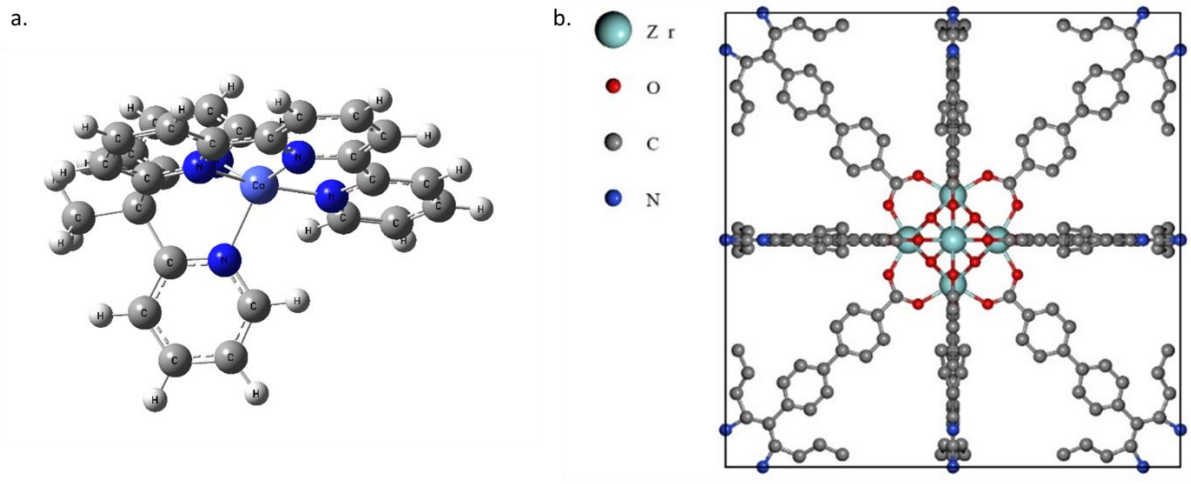

Figure 1. (a) DFT optimized structure of Co^{+} from calculations using ωB97X-D functionals and CH_3CN solvent adapted from coordinates in [14] and (b) unit cell of TNP-MOF adapted from CDCC structure in [15]

Also, DFT particularly Time-Dependent Density Functional Theory (TD-DFT) has been used to understand the light absorption properties of Tetrakis (4-carboxbiphenyl) napthoporphyrin linker in metal organic frameworks (TNP-MOF) used in photosensitive CO_2RR [16]. The unit cell of TNP-MOF is illustrated in **Figure 1**. The TDDFT calculated absorption spectrum showed that the Q-band of TNP was much higher than other ligands studied and which was in agreement with what was observed experimentally from steady-state absorption spectra using Ultraviolet photoelectron spectroscope. Ditto applied to the gaps between HOMO and LUMO orbitals which was in concordance with the change trend observed in band positions experimentally. A linear proportional relationship was observed between the extension of π-conjugated system of the linker and the delocalization of the π conjugated electron leading to a red shift in absorption of the linkers. The theoretical results suggested that the energy levels of the linkers studied in this work [16]were feasible for the reduction of CO_2 into HCOOH.

Another relatively new computational method besides DFT that is applied in photosensitive CO_2 reduction is the application of Artificial Intelligence (AI) tools such as Machine Learning (ML) and Deep Learning (DL). In a recent work, Li et al [17] applied an ML classification algorithm to predict catalytic performance of MOFs on a dataset derived from about 100 published experimental papers. This work discovered that the following metals -Mn, V, Cu, Ni, Zr and Y alongside these ligands (tactmb, tdcbpp, TCPP and H_3L) could be combined to make 24 MOFs which are potential catalyst for CO_2 reduction. This work tested and compared five ML algorithms- Support Vector Classifier (SVC), K-Nearest Neighbor (KNN), Decision Trees (DT), Stochastic Gradient Descent (SGD) and Neural Network (NN) on 1311 hypothetical MOFs. The SVC and NN had the best metric scores with respect to performance from their F1- score and accuracy. The implementation of AI would help facilitate the discovery of new photosensitive materials capable of CO_2 reduction. However, it is important to note that computational techniques serve a complementary purpose to aid experimental work in material discovery.

3. Fundamental mechanism of the photocatalysis

Photocatalysis is considered to be an artificial form of photosynthesis whereby solar energy is harvested for the conversion of CO_2. The pioneer work regarding photocatalysis was reported by Halmann and his group using p-GaAs as photo-

electrocatalyst over a cathodic bias [18]. The reduction of CO_2 by photocatalysis is similar in mechanism to the natural photosynthesis, which can be explained using three separate but linked steps: (i) the absorption of solar energy (ii) the separation of charges and (iii) surface redox reaction [19]. The light absorption induces light excited 'photo-hole and photo-electron' formation in a light harvesting material (semiconductors) [20]. First, a light energy of equal or greater energy is supplied to promote electron(s) from the photocatalyst valence band (VB) to its conduction band (CB) to produce photo-hole (h^+) and photo-electron (e^-), respectively and the effectiveness of the semiconductor depended on its design in terms of band gap energy [21]. The second stage are, however, characterized with different processes, like transfer of photogenerated charges to the surface, in-band transitions, electron-hole recombination and others [22]. The last stage describes the participation of the surface charges in redox reaction, whereby the photo-electrons in the CB induces the reduction of CO_2 to various products. Also, before reduction of CO_2 takes place, the mechanism of reduction entails the coordination of the molecule (CO_2) to photocatalyst metal center for activation and metal adduct formation and then followed by the transferring of proton to metal adducts intermediates to form different products, depending on the nature of photocatalyst used [23].

Thermodynamically, due to shorter period of relaxation of electron-hole, it is less likely to have equilibrium between the forbidden bands (energy difference between the bottom of CB and top of VB) than an internal equilibrium existing within the energy levels [24]. Representing the electronic states in equilibrium (quasi-equilibrium states) as given in equations 1, 2 and 3, it is possible deduce the thermodynamic feasibility of redox reaction on catalyst surface [25]:

$$F_n = CB + KTln\frac{n}{Nc} - - - - - - - - - - - - - - - - 1$$

$$F_p = VB + KTln\frac{p}{Nv} - - - - - - - - - - - - - - - - 2$$

$$\Delta G = -\left|F_n - F_p\right| = -E_g - KTln\frac{pn}{NcNv} - - - - - - - - - - 3$$

VB and CB have their usual meanings while Nv and Nc means effective density of states for VB and CB, respectively. K, *p*, and *n* represents Boltzmann constant, hole and electron concentrations, respectively. Inferentially, according to equation 3, when

the difference between pseudo-fermi levels, ΔG becomes more negative and the photocatalytic redox reaction is more spontaneous. Furthermore, the position of CB dictates CO_2 reduction thermodynamics. **Figure 2** reveals an overview of the tendency as well as the standard potentials of different types of semiconductors for production of value-added-products from CO_2 reduction.

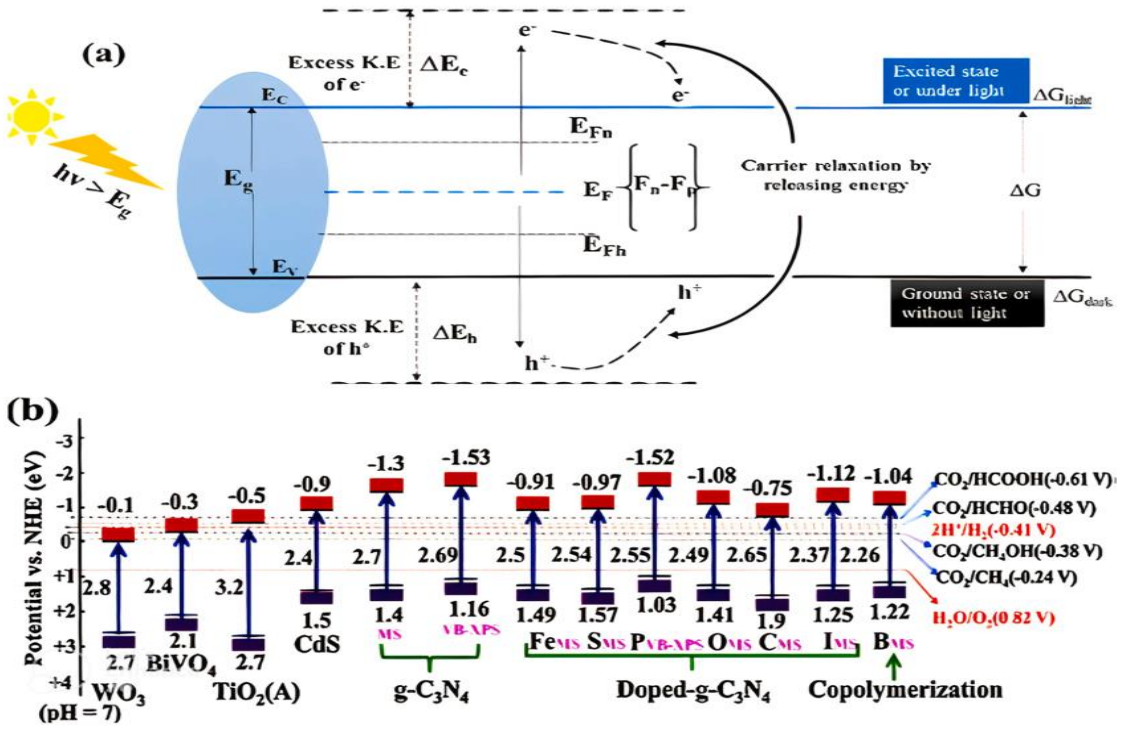

Figure 2: ΔG and semiconductor thermodynamics with and without illumination (a); semiconductor band potential and their applicability for forming value-added-products (b). Adapted with permission from [26]. Copyright (2018) Elsevier

4. Metal-complex photocatalysts

Experimentally, the application of metal-complex photocatalysts has attracted attention and research in abating CO_2 and findings revealed that it is possible to precisely control the functionality of metal complexes, including their photophysical, electrochemical, and catalytic properties, by designing them at the molecular level [27]. As such, the photocatalytic activity of metal complexes for CO_2 reduction into hydrocarbon fuels has been explored and reported in various previous studies. For example, Hawecker and colleagues[28] for instance, used [fac-Re(bpy) $(CO)_3Cl$] (bpy = 2,2′-bipyridine) to demonstrate one of the first metal complexes as an effective homogeneous catalyst for selective and sustained photochemical reduction of CO_2 to CO in 1986. The researchers

measured a quantum yield of 14% and a faradic efficiency of 98% in the presence of additional Cl ions. Photocatalytic CO_2 reduction using metal complexes has evolved since then, and new viewpoints have fundamentally transformed the field of study.

It is important to mention that a photosensitizer and a CO_2-reduction catalyst are the two main components of the bulk of contemporary metal-complex-based homogeneous photocatalytic systems. As an illustration, Kumagai and his colleagues [29] recently developed a mixed system of a ring-shaped Re(I) trinuclear complex as a photosensitizer and fac-[Re(bpy)$(CO)_3${$OC_2H_4N(C_2H_4OH)_2$}] as a catalyst which selectively photocatalyzed CO_2 reduction to CO with the highest quantum yield of 82% and a turnover number (TON) of over 600. The group also investigated a Cu(I) dinuclear complex as a photosensitizer and fac-Mn(bpy)(CO)3Br or Fe(phen)2$(SCN)_2$ as catalysts (**Figure 3**). The total quantum yield of CO and HCOOH from CO_2 was 57% with TON $_{CO + HCOOH}$ >1300 against fac-Mn(bpy)(CO)3Br] and the quantum yield of CO recorded against Fe(phen)2$(SCN)_2$ was 7% with TON_{CO} >270. In another example, Takeda and co-workers [30] designed CO_2 reduction photocatalysts employing $[Cu_2(P_2bph)_2]^{2+}$ (CuPS) (P_2bph = 4,7-diphenyl-2,9-di(diphenylphosphinotetramethylene)-1,10-phenanthroline) as a redox photosensitizer and fac-Mn(X_2bpy)$(CO)_3$Br (Mn(4X)) (X2bpy = 4,4′-X_2-2,2′-bipyridine (X = −H and −OMe) or Mn(6mes) (6mes = 6,6′-(mesityl)2-2,2′-bipyridine)) as the catalyst. The CO_2 reduction process was 95% selective, the overall quantum yield of CO_2 reduction products was 57%, and the Mn catalyst had a TON >1300.

However, because such transfer necessitates physical contact between the photosensitizer and the catalyst, electron transfer from the one-electron-reduced species to the catalyst is frequently the rate-determining step in two-component homogeneous systems like these. Despite the fact that these metal complexes demonstrated impressive photocatalytic activity for CO_2 reduction, studies have revealed that metal complexes suffer a setback when it comes to inducing a continuous selective reaction in a mixture of reactants and products due to the different reaction conditions required for CO_2 reduction.

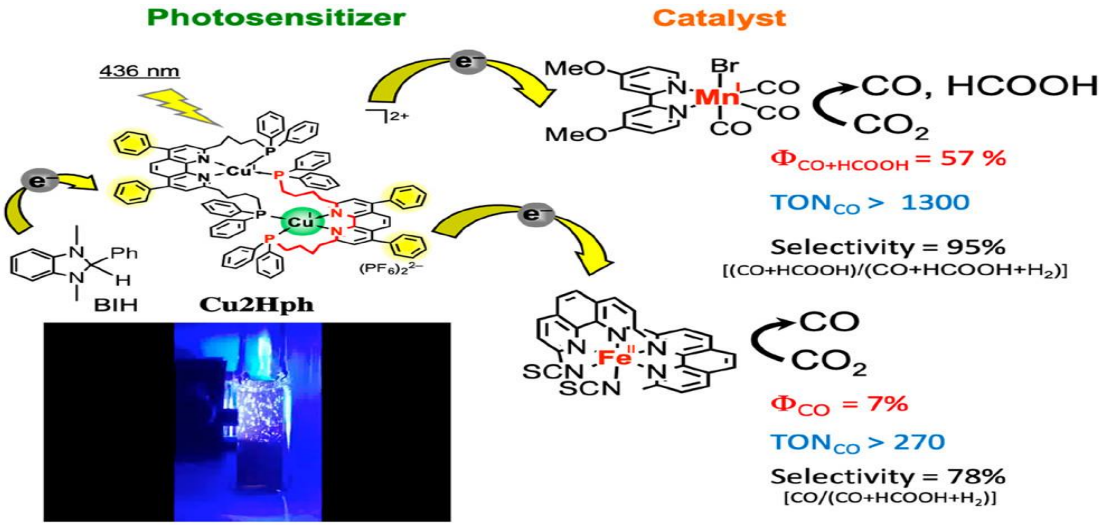

Figure 3. Mechanism of photocatalytic reduction of CO_2 by Cu_2Hph as photosensitizer and fac-Mn(MeO-bpy)$(CO)_3$Br or Fe(phen)2$(SCN)_2$ as catalysts. Adapted with permission from [29]. Copyright (2022) American Chemical Society

5. Metal Oxide Photocatalysts

Fujishima and Honda [31] first demonstrated the use of metal oxides as a photocatalyst for CO_2 reduction in the 1970s, using a rutile-TiO_2-based photoelectrochemical cell for water splitting. Since then, several studies have been published that use various approaches to improve the photocatalytic performance of semiconductors for CO_2 reduction, such as the addition of cocatalysts or other surface modifications. From the available studies, semiconductors offer superior photo-oxidation activity, stability and recyclability [32]. One conspicuous advantage of semiconductor photocatalysts compared to its counterpart (metal complex) is that it can use water as an electron donor under the conditions employed for photocatalytic reduction of CO_2 [33]. However, the reduction of CO_2 in an aqueous solution is limited by low quantum efficiency due to preferential H_2 production under visible light.

Several metal oxide semiconductors have been employed in the recent decade to reduce CO_2 emissions by employing water as an electron donor [34,35]. The huge band gap, however, prevents it from using visible or solar radiation. For instance, Guo and co-workers [36] demonstrated photoreduction capability of $AgTaO_3$ for CO_2 reduction utilizing H_2O as an electron source. $AgTaO_3$ with Ag cocatalyst loaded by photo deposition demonstrated the maximum activity for CO generation among those with Pt, Rh, or Cu cocatalysts after adjusting the synthetic conditions and performing different

surface modification with variety of cocatalysts. When core/shell structured metal nanoparticles were combined with Cr_2O_3, $AgTaO_3$ photocatalyst demonstrated CH_4 evolution activity in photocatalytic CO_2 conversion, indicating that Cr_2O_3 species accelerated the hydrogenation process of CO_2 reduction. The results of this study showed that cocatalyst decoration changed conversion products and was crucial for multielectron photoreduction of CO_2. In another study, Liu and co-researchers [37] presented a way for improving the solar fuel generation rate of TiO_2 by loading cocatalysts, specifically bimetallic Cu-Pt and CuO, through two-step photodeposition procedures. The photocatalytic H_2 generation rate of the Cu-Pt/TiO_2-CuO sample under simulated sunlight conditions is 173.7 µmol/g.h. For photocatalytic CO_2 reduction by water, the Cu-Pt/TiO_2-CuO sample displays the release of H_2, O_2, CO, CH_4, and CH_3OH, with CO being the predominant reaction product. The O_2 and CO yields for LED-405 and LED-425 are typically 4.2 and 6.2 and 2.1 and 3.2 µmol/h.g, respectively; the CO_2-to-CO conversion ratios for separated carriers are 73.8 and 76.19%.

MXene materials have recently been discovered to be ideal co-catalysts and/or catalyst supports for improving semiconductor performance for photocatalytic CO_2 reduction. According to a recent review work carried out by Shen and co-workers [38], the inclusion of M-Xene as catalyst support has been discovered to improve the separation of electrons and positive holes, improve the light absorption and photochemical effect, enhancing the adsorption and activation of CO_2 and inhibition of photo-corrosion. In one of the earlier computational studies of Mxene as a potential catalyst/cocatalyst for CO_2 reduction, Zhang et al. [39] used first-principles simulations to examine CO_2 catalytic reduction processes at oxygen vacancies in three Mxene (Ti_2CO_2, V_2CO_2 and $Ti_3C_2O_2$). The group considered four potential single-carbon organic compounds (HCHO, CH_3OH, CH_4, and HCOOH). Their findings show that oxygen vacancies at the surface of Mxene play a crucial role in the reduction of CO_2. They, therefore, proposed that sufficient oxygen vacancies can be introduced to the MXene surface by CO and H_2. Ti_2CO_2 has the best catalytic performance for the reduction of CO_2 among the three types of MXene. This computational investigation gives a new insight into the emerging application of Mxene in the area of photocatalytic reduction of CO_2 into hydrocarbon fuels which later come to manifestation.

In a recent paper, for example, Li and co-authors [40] reported a ternary material containing MXene as an efficient photocatalyst (**Figure 4**). According to the group findings, bronze TiO_2 (TiO_2(B)) Schottky junction composites were created using Ti_3C_2 MXene and electrostatic self-assembly. The surface of the TiO_2(B)/Ti_3C_2 MXene was then further covered with Ag_3PO_4 quantum dots through in situ self-growth, and Ag_3PO_4 joined TiO_2(B) and Ti_3C_2 MXene to create heterojunctions and Schottky junctions, respectively. These functional connections worked together to create the photocatalyst TiO_2(B)/Ti_3C_2 MXene/Ag_3PO_4. Under the synergistic influence of these functional connections, the mobility and quick separation capabilities of the photogenerated electron-hole pairs of the composite photocatalyst were greatly increased, and the recombination of photogenerated electron-hole pairs was successfully prevented [41]. Additionally, light absorption performance has been increased. As a result, the composite photocatalyst demonstrated exceptional photocatalytic activity.

Furthermore, in the search for effective and eco-friendly semiconductor photocatalysts for the reduction of CO_2 to different hydrocarbon fuels, some scientists have incorporated biological enzymes into semiconductors [42]. For example, White et al. [43] showed that [NiFe] CODH II from *Carboxydothermus hydrogenoformans* can be effectively activated by light to reduce CO_2 to CO. To do this, the researchers developed a hybrid photosystem combining CdSe/CdS dot-2in-rod nanocrystals and CODH II. The use of a low-potential redox mediator to aid electron transport resulted in quantum yields of up to 19% and turnover frequencies of 9 s^{-1}. These findings establish a new standard for effectively lowering CO_2 emissions using photocatalytic enzyme systems.

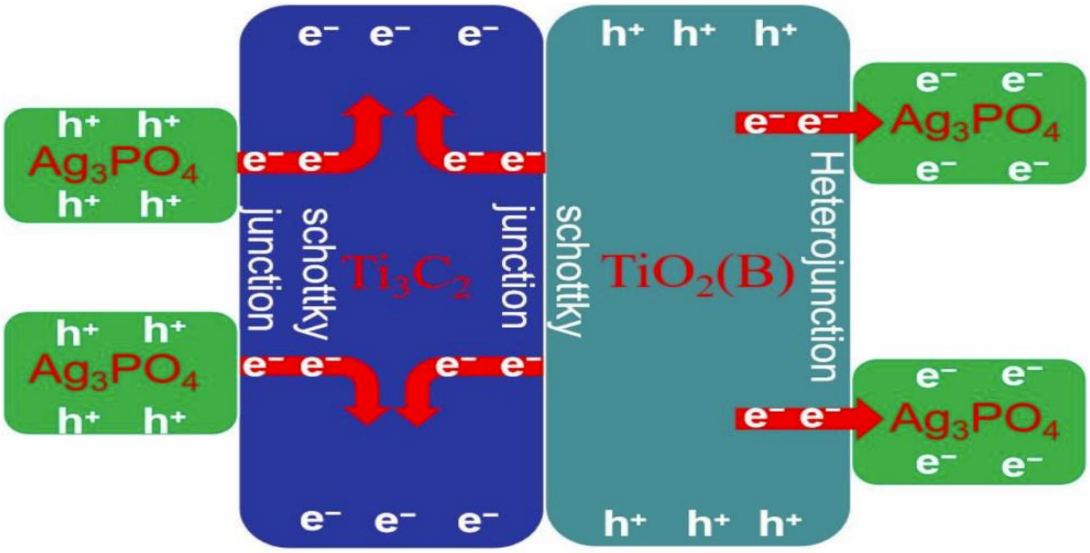

Figure 4. Mechanism of enhanced photocatalytic properties of semiconductor by M-Xene. Reproduced with the permission of [40]

6. Metal-Organic Framework Photocatalysts

Metal-organic frameworks (MOFs) are described as three-dimensional structures having multiple linkers as organic molecules and inorganic nodes [44,45]. Fundamentally, photocatalysts are semi-conducting materials, in which upon irradiation, electrons (e^-) in the material are excited from the valence band to the conduction band[46,47]. The migration of electron, due to the reception of light energy, usually leave behind a positive vacant hole (h^+) in the valence band part of the photocatalyst as shown in **Figure 5**[48]. Here, the electron moves from HOMO (valence band) to LUMO (conduction band) and this serves as the basic feature of any semi-conducting substance like MOFs. To function effectively as a catalyst, the interfacial electron transfers as well as the separation of the e^- and h^+ requires optimization [49], else the separated charges may recombine and thus, resulting in energy-wasting process [50–52].

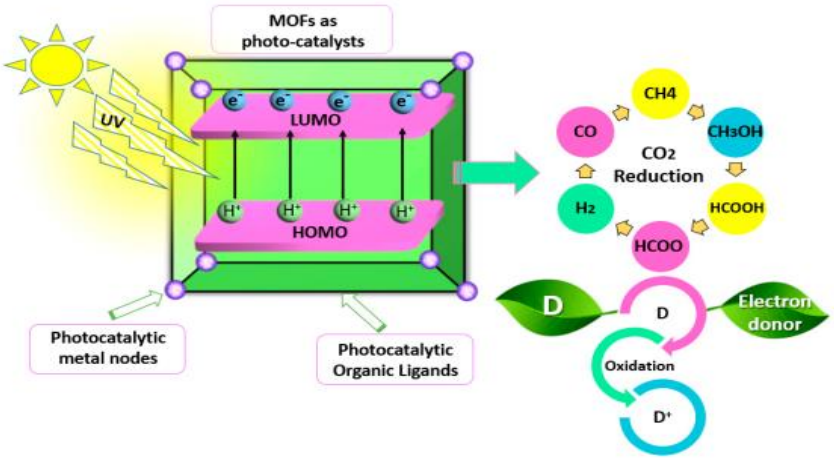

393

394 **Figure 5.** Separated charges on MOF for CO_2 photo-reduction process [48]

395 In chemical and petrochemical industrial processes, zeolites have found catalytic
396 application sequel to its chemical and thermal robustness, in addition with the easy
397 formation of the acidic site [53]. Zeolites can be synthesized and it can be found
398 occurring naturally. In recent years, attention has shifted towards the use of synthetic
399 form as the size and shape can be sufficiently altered to give the desired materials by
400 simply adjusting synthesis condition like time length, temperature required for
401 synthetic zeolite formation and Si/Al ratio [54,55]. Characteristically, zeolites have
402 negatively charged tetrahedral aluminoxy which is loosely attached to the zeolite
403 skeletal structure and commonly counter-balanced by Group 1A or 2A elements, like
404 Ca^{2+}, Na^{+}, Mg^{2+} and so on [56]. Zeolite basicity is enhanced when more aluminum
405 atoms are present in aluminosilicate framework; and the more the basicity of zeolite,
406 the high the capacity to capture CO_2 [57].

407 Photochemically, zeolites are inert, behave as insulating material and are therefore not
408 excited when irradiated [58,59]. When compared, MOFs are also descried as poor
409 conductors due to the presence of organic ligand p-orbital conjugation, however,
410 scientists have attempted to incorporate electrical conductivity into MOFs following the
411 achievement of Allendorf in applying MOFs as microelectronic material [60]. MOFs
412 are characterized as hybrid materials with tunable structure which confers on them
413 versatility than any organic or inorganic semi-conducting materials [60,61]. The light
414 absorbing portion of MOFs can be linked to the organic linkers that are connected to
415 the inorganic part of MOFs (metal nodes); here, the organic linkers are receptive to
416 light and induce the activation of quantum dots [62]

The photocatalytic properties are exhibited, just as in the case of semiconductors, via ligand-to-metal-charge transfer (LMCT) and $\pi \rightarrow \pi^*$ electron transition in organic linkers in the visible (400-800 nm) and ultraviolet (200-400 nm) region of the electromagnetic spectrum, similar to semiconductors [63]. Pure zeolite, on the other hand, are only capable of absorbing light at wavelength lower than 220 nm [64]. Garcia et al. investigation into the property of MOFs confirmed the semiconducting features of MOFs via LMCT which resulted into separation of charges to form e^- and h^+ [65]. They found that photoinduced electron transfer processes to viologen produces the corresponding viologen radical cation, while holes of MOF-5 were effective at oxidizing N,N,N′,N′-tetramethyl-p-phenylenediamine. The detection of delocalized electrons was observed by using laser flash photolysis technique, revealing microseconds residence time of electrons in the conduction band (CB). Findings have revealed that, besides LMCT, $\pi \rightarrow \pi^*$ in MOFs ligand is suggested as a feasible mechanism for the semiconducting properties of some MOFs [66,67].

6.1 CO_2 capture by MOFs

The simultaneous capturing and storage of carbon dioxide as well as its transformation to fuels are now the primary focus of research in CO_2 reduction, in order to tackle the global climate change [68–71]. The dominant capturing approach is via chemisorption onto the functionality on the MOFs. Flaig and coworkers observed that there was 2.3 times increment in the capturing of CO_2 by IR-MOF-74-III-CH_2NH_2 at lower CO_2 pressures and it as ascribed to promotion of chemisorption of CO_2 due to the presence of two alkyl-amines per organic linker in the MOF [72]. **Figure 6** shows a typical mechanism for CO_2 capture by IR-MOF-74-III-$(CH_2NH_2)_2$. The three basic approaches employed by using MOFs for the reduction of CO_2 emission coming from fuel combustion in power plants oxy-fuel combustion, post-combustion and pre-combustion capturing [48] The choice of any of the aforementioned methods solely depends on a number of factors like CO_2 concentration and its partial pressure in flue gas, and the merits and demerits of each of the approach. The comparison of the approaches is presented in **Table 1.**

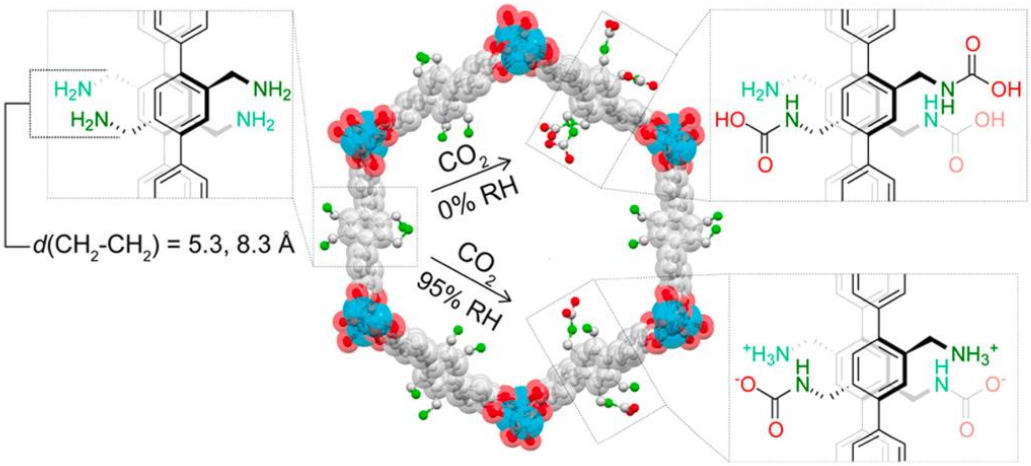

Figure 6. Schematic representation of mechanistic CO_2 capture by IR-MOF-74-III-$(CH_2NH_2)_2$ (Mg2(2′,5′-bis(aminomethyl)-3,3″-dioxido-[1,1′:4′,1″-terphen-yl]-4,4″-dicarboxylate) Adapted with the permission [72]. Copyright (2017) Elsevier

Table 1. Merits and demerits various approached for CO_2 capture [48]

Merits			
Entry	Post-combustion	Pre-combustion	Oxy-combustion
1.	Frequently employed methods in CO_2 capture	Less volume of water is required in this process, compared to post-combustion method	No need for onsite-operation and can fit into an existing power plant
2.	Plant efficiency is enhanced and CO_2 emissions reduced due to development of powdered coal systems	Synthetic gas can find application in powering turbine cycle	It requires a low-cost to capture CO_2. For instance, more than of CO_2 can be captured by this low-cost approach
3.	Research and developments are ongoing to further improve the adsorption capacity of adsorbents and capturing instrument	This approach requires a low-energy for CO_2 capture compared to other methods	Pollutants released by this approach are at low-cost.
4.	Suitable for current and future coal-powered power plants	Often applied in industries	Large volumes of steams are generated

Demerits			
Entry	Post-combustion	Pre-combustion	Oxy-combustion
1.	The efficiency is negatively affected due to steam extraction that reduce the flow into turbine	Supporting systems extensively needed	Scaling-up requires further findings or experiments
2.	For high CO_2 capture, this method requires large volume of water and a high circulation volume.	Only suitable for new power plants	Leakage of CO_2 is most possible
3.	At ambient condition, the partial pressure of CO_2 is low	In this method, energy is majorly lost	High energy is needed
4.	Reduction in efficiency as a result of application of amine technologies in this approach	Expensive to procure equipment	Overall, it is not cost-effective

Previous studies have reported the features of MOFs that are suitable for CO_2 capture. For instance, it was mentioned that MOF for CO_2 capture should have enhanced porosity, CO_2 adsorption capacity and selectivity [73]. Also, the authors mentioned that a perfect material for CO_2 capture should possess an extremely reduced uptake ability for other gasses like nitrogen and methane, when compared with its adsorption capacity for CO_2 [73] According to Kang et al. in any industrial process involving the separation of gases, it is usually a challenging task. However, MOFs have proven to be suitable materials to be used in gas separation applications in industries [74]. MOF materials' unique structural and chemical features, such as pore porosity, open metal sites, and polar functional groups in the pore channel size, have informed their effectiveness in capturing CO_2 [75]**Table 2** presents some examples of MOFs, their CO_2 uptake capacity and operating conditions.

Table 2. A compiled list of some MOFs and the adsorption capacity for CO_2

Entry	Type of MOFs	Operating conditions	CO_2 adsorption capacity	References
1.	UMCM-1-NH_2-	T=25 ^oC; P= 18 bar	19.8 mmol/g	[76]

	MA			
2.	A core–shell MOF	T=0 ^{o}C; P= 1 bar	41 mmol/g	[77]
3.	HCM-$Cu_3(BTC)_{2-3}$	T=25 ^{o}C; P= 1 bar	2.8 mmol/g	[78]
4.	(ZIF-20)	T=0 ^{o}C; P= 760 Torr	70 mL/g	[79]
5.	Zn(adc) (4,40-bpe)$_{0.5}$	T= -78.15 ^{o}C; P= 1 p/p	130 mmol/g	[80]
6.	Zn(II)-based MOFs	T=25 ^{o}C; P= 1 bar	9.2 mmol/g	[81]
7.	(PCN-5)	T = -78.15 ^{o}C; P = 760 Torr	210 mg/g	[82]
8.	SNU-110	T = 78 ^{o}C; P = 1 bar	6 mmol/g	[83]
9.	$Cu(dhbc)_2$ (4,40-bpy)	T=24.85 ^{o}C; P=0.4~8 atm	70 mL/g	[84]
10.	Cu(pyrdc)(bpp)	T = -78.15 ^{o}C; P = varies	varies	[85]
11.	MOF with PEI	T = 78 ^{o}C; P = 0.15 bar	4.2 mmol/g	[86]
12.	[$Ni(bpe)_2$ $(N(CN)_2)$] $(N(CN)_2$	T= -78.15 ^{o}C; P = 1 p/p	35 mL/g	[85]
13.	Cu(bdc) (4,40-bpy)$_{0.5}$	T=24.85 ^{o}C; P = 0.10 MPa	70 mL/g	[84]
14.	MIL-53 with BNH_x	T = 0 ^{o}C; P= 1 bar	4.5 mmol/g	[87]
15.	(MIL-53)	T = 30.85 ^{o}C; P = 20 bar	7.5 mmol/g	[88]
16.	NJU-Bai12	T = 0 ^{o}C; P = 20 bar	28.3 mmol/g	[89]
17.	Cu(fam) (4,40-bpe)$_{0.5}$	T = -78.15 ^{o}C; P = 760 torr	100 mL/g	[90]

6.2 The utilization of MOFs in CO_2 photoconversion

Photo-conversion also known as photocatalysis are basically catalytic reactions that occurs under the influence of sunlight [91]. Metal organic frameworks which comprise of a metal linked to organic ligands to form a well-coordinated network are often used as photocatalyst for CO_2 conversion due to their promising potentials to solve environmental problems associated with CO_2 release. Other conventional

photocatalysts such as semiconducting compounds (e.g., Zn_2GeO_4, Zn_2GeO_4, CdS) that incorporates a metal-zeolite framework have lower performance due to lower efficiency of charge separations, surface area and weak adsorption capacity for CO_2 [92]. In contrast, MOFs are known to be a good material for CO_2 conversion because the framework supports high absorption of photons due to electrophilic aromatic polymeric species present in the structure following electron transfer from the organic ligands to the central atoms thus leading to charge separation of localized excitons [64,93]. Another thrilling discovery is that the adsorptive potentials of MOFs can be enhanced by utilization of light harvesting components which can be synthesized using a visible light-sensitive metal like iron (Fe) [94]. However, this might affect their adsorptive capacity and CO_2 selectivity in aqueous media, gases and acid [95]. Organic components or linkers used for light harvesting responds to light due to f actors like functionality e.g., 2aminoterephthalic acid, or inclusion of photoreactive met alloligands[94,96].

Furthermore, due to the porous structure of MOFs, photosensitive materials can be incorporated into the cavity's framework which is quite difficult to achieve in other semiconductor catalysts such as Zn_2GeO_4, CdS since the photosensitive sites are dispersed on the exterior surface of the complex instead of the structure's cavity [92,97]. In addition to this, the immobilization of the photoactive sites in the linker coupled with the cavity structures and metal mode of MOFs makes them a suitable candidate for a lot of applications especially when designing smart materials that are sensitive to external stimuli. This potential characteristic makes them more versatile in use compared to zeolites[92,98]. Even though several efforts have been put into the optimization of the photolytic performance of MOFs, some milestones are yet to be covered.

6.2.1 Mechanism of CO_2 photo-reduction by MOFs

CO_2 photo-reduction takes place in the presence of light (200-800 nm). This reduction can lead to the formation of CH_4, CO, HCHO, and CH_3OH, depending on the reduction potential [75] (see **Table 3**). The photo-reduction of CO_2 occurs in a series of steps as follows. The CO_2 pollutant is adsorbed on a photocatalyst like MOFs, there is formation, separation and transportation of charge carriers (photo-hole and photoelectron) and the surface species (CO_2) react with the formed charges to form various products depending on reduction potential needed for a particular product to be

formed [99,100]. As a result of the interaction of the photo-hole and photo-electron forms, photocatalysts with low bandgap and high redox potential are suitable for CO_2 photo-transformation. With the use of MOFs, light is first absorbed by the photocatalyst (MOFs) resulting in charge (photohole-photoelectron) separation via excitation of electron from the highest occupied molecular orbital of organic linkers in MOFs (HOMO) to the lowest unoccupied molecular orbital of organic linkers in MOFs (LUMO) [101]. Subsequently, the adsorbed CO_2 consumes the electrons formed (in the LUMO) to form different categories of value-added products such as CO, CH_4, CH_3OH and HCOOH.

Table 3: Various standard reduction potentials of CO_2

Entry	Reduction potentials	Normal hydrogen electrode vs reduction potential (V)
1.	$CO_2 + 8H^+ + 8e^- \rightarrow HCHO + H_2O$	-0.24
2.	$CO_2 + 4H^+ + 4e^- \rightarrow HCHO + H_2O$	-0.48
3.	$H_2O \rightarrow 1/2O_2 + 2H^+ + 2e^-$	+0.41
4.	$CO_2 + 6H^+ + 6e^- \rightarrow CH_3OH + H2O$	-0.38
5.	$CO_2 + 2H^+ + 2e^- \rightarrow CO + H_2O$	-0.53
6.	$CO_2 + 2H^+ + 2e^- \rightarrow HCOOH$	-0.61
7.	$CO_2 + 2H^+ + 2e^- \rightarrow HCOO^-$	-0.49

6.2.2 Challenges of MOFs synthesis and application

The chemical and thermal instability of MOF photocatalysts during synthesis is a significant issue. At temperatures above 250^{o}C, several MOFs break down during synthesis. Because of interactions with species that contain nucleophiles in the synthetic chemicals, the network structure may become unstable [102,103]. A few examples of such nucleophilic substances are amines and alkoxide. The potential for photochemical instability that results from extended exposure to the metal-organic network to irradiation and causes photo-oxidation of the organic moiety of the

framework is another aspect that hinders MOFs' performance. Therefore, it is essential to pay attention to this material's photostability when exposed to light [64]. This might be done by running a timed-control experiment to determine the exact time allowance for the MOFs of interest, then utilizing spectroscopic methods and the X-ray diffraction (XRD) method to confirm the stability.

7. Z-scheme photocatalysts

The natural process of photosynthesis, in which photogenerated electrons are carried through a Z-scheme mode, allows green plants to efficiently convert CO_2 and H_2O to O_2 and carbohydrates [104]. An artificial Z-scheme photocatalyst with higher potential for generating high photocatalytic performance in CO_2 reduction is one that was inspired by this natural photosynthesis process [105]. The artificial Z-scheme photocatalyst usually consists of two semiconductors. The roadmap for the historical evolution of Z-scheme photocatalysts [106] and different charger transfer routes of Z-scheme family are presented in **Figure 7**. In summary, Z-scheme photocatalysts can be divided into three generation [105] (1) First generation: traditional Z-scheme photocatalysts in redox ion pairs such as $Fe3^{+}/Fe^{2+}$ is used as medium for charge carriers (2) Second generation: all solid state Z-scheme photocatalysts in which electron conductor such as platinum nanoparticles is employed to serve as charge transfer medium (3) Third generation: direct Z-scheme photocatalysts, in which the charge carrier transfer is mediated by an internal electric field rather than a third party and a direct contact between two semiconductors is ensured.

It is important to mention that high stability for water oxidation is one benefit of semiconductors but low selectivity for CO_2 reduction is one major drawback (accompanied with H_2 evolution). A molecular metal complex, in contrast, has moderate ability for oxidation process under the condition of photocatalytic CO_2 reduction but good selectivity for photo- and electrochemical CO_2 reduction. With these advantages and disadvantages of metal complexes and semiconductors in photocatalytic CO_2 reduction systems in mind, it seems likely that a hybrid system with a metal complex and a semiconductor acting as the reduction and oxidation centers, respectively, could function as an efficient visible-light photocatalyst for CO_2 reduction with high selectivity using water as the electron source. In aqueous environments, the performance of such metal-complex/semiconductor hybrid systems could be improved

by anchoring water-insoluble metal-complex (photo)catalysts to solid surfaces to avert unfavorable aggregation [107].

This section focuses on scientific literature on two semiconductors and hybrid photocatalysts for CO_2 reduction. One of the earliest research works on Z-scheme (metal-complex/semiconductor) was reported by Sato and co-workers [108] in the year 2015. The team demonstrated a semiconductor/metal-complex hybrid photocatalyst for selective CO_2 reduction, employing the metal complex catalyst $[Ru(dcbpy)_2]Cl_2$([Ru-dcbpy]) (dcpy =4,4' -dicarboxy-2,2' -bippyridine) with electrocatalytic CO_2 reduction. The Z-scheme approach, at least in theory, can solve both the poor reduction performance of semiconductor photocatalysts and the poor oxidation ability of metal-complex photocatalysts. Because less energy is needed to drive CO_2 reduction and water oxidation than in a one-step photoexcitation system, a Z-scheme system can utilize a wider range of visible light. Both the metal complex and the semiconductor components have a significant impact on the photocatalytic performance of such two-reaction schemes. Therefore, the development of metal complexes and semiconductors is crucial. **Table 4** lists some of the recently developed metal-complex/semiconductor hybrid systems for CO_2 reduction using visible light photocatalysis and photo-electrochemistry.

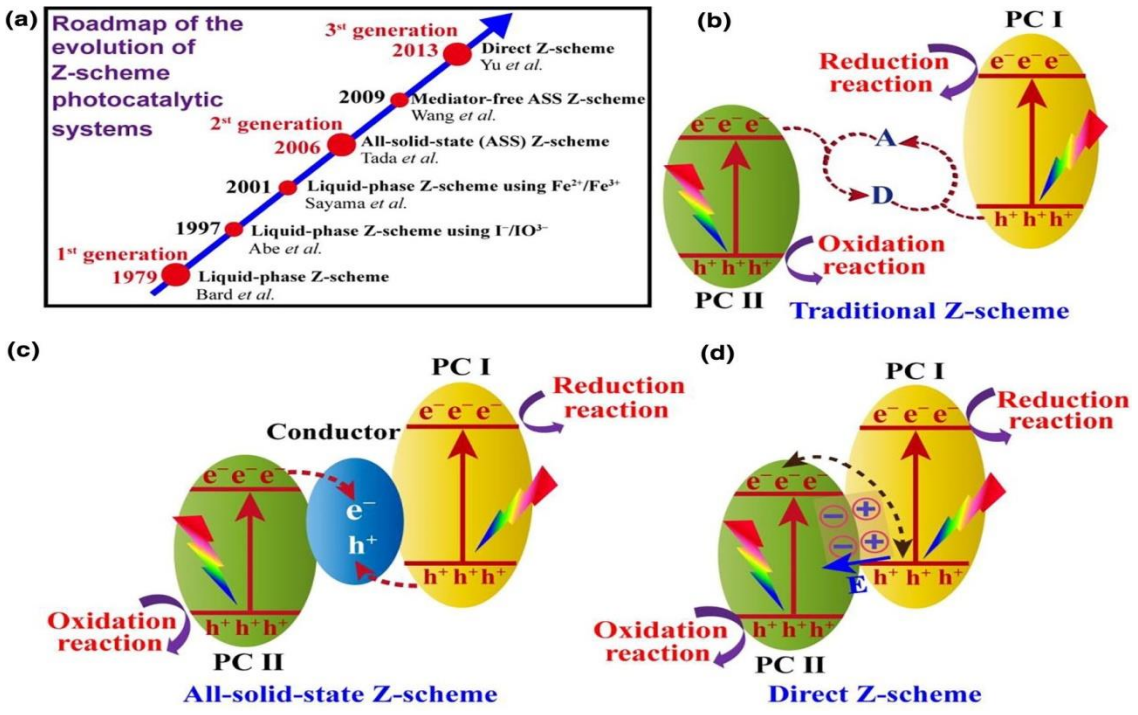

Figure 7. (a) Roadmap for the of evolution of Z-scheme photocatalysts (b) Traditional Z-scheme charge transfer mechanism (c) All-solid-state Z-scheme charge transfer mechanism (d) Direct Z-scheme charge transfer mechanism. Adapted with the permission [105] . Copyright (2018) Elsevier.

Table 4. Z-scheme metal complex/semiconductor hybrid system for the reduction of CO_2 by photocatalysis and photoelectrochemistry driven by visible light

Z-scheme Photocatalysts	**Cocatalysts**	**Conditions**	**Yield (%)**	**Catalyst dose (mg)**	**Main product**	**Remarks**	**Ref.**
TaON and Ta/N-co-doped TiO_2 in conjunction with a binuclear Ru (II) complex, GaN:ZnO solid solutions	Ag	300W xenon lamp; λ>400 & 365 nm; 15h; pH:6.4	-	4	Hydrogen and formate	It demonstrates the huge potential of band-tunable mixed-anion semiconductors as components of Z-scheme hybrid photocatalysts for CO_2 reduction via visible light.	[109]
Copolymerized carbon nitride paired with Ru (II) complex	polymer	300W xenon lamp; λ>500 nm; 5h	98	20	Formic acid	The study unmistakably demonstrated that, even without the need for the labor-intensive postsynthesis modifications typically used to increase electron density, a straightforward modification of a bulk	[110]

						semiconductor through the copolymerization approach becomes another efficient way to increase the photocatalytic activity of the hybrid photocatalyst.	
Ru-complex Ta_2O_2(N-Ta_2O_5: nitrogen doped Ta_2O_5) hybrid	NH_3	500W xenon lamp; λ>390 - 750 nm; 15h; pH:5-6		10	Carbon monoxide and formic acid	The research contends that NH_3 adsorption on the surface facilitates electron transport from the Ta_2O_5 to the Ru-complex. Additionally, it appears from the calculations done in this work that the replacement of NH groups for surface oxygen atoms causes Ta2O5's absorption band edge to shift red, but the CBM to shift upward just slightly	[111]
Macrocyclic Co(III) on three different semiconductor surfaces	No	mercury lamp; λ>420 nm; 5h		10		Because N-Ta2O5-based hybrid photocatalysts lack surface functionalities (such as hydroxyl groups) necessary for the molecular deposition of cobalt complexes, they exhibit poor activity.	[112]
Mesoporous	Polym	300W	60	8	Carbon	To achieve photocatalytic	[11

carbon nitride with polymeric cobalt phthalocyanine catalyst	er	xenon lamp; λ>500 nm; 5h			monoxide	CO_2 conversion, the in situ polymerization of the phthalocyanine is essential because it enables control over the catalyst loading.	3]
Mn-immobilized TiO_2 hybrid (OrgD-|TiO_2|-**MnP**)	Dye	60W LED lamp; λ≥400 nm; 23h	> 99	10	Formate and carbon monoxide	The amount of MnP loaded onto the surface of TiO2 was discovered to be a key factor in controlling the product selectivity (HCOO-/CO)	[114]
Ir X^+ immobilized on ReC anchored TiO_2 hybrid catalyst	Ir (III) complex	60W LED lamp; λ>400 nm	-	10	Carbon monoxide	This study establishes that Ir-X+ can function in solution as an efficient and reliable photosensitizer for the CO_2 reduction based on the TiO_2/ReC binary catalyst. It also suggests that the structure-reactivity relationships investigated in this study may provide a strategic basis for the molecular design of Ir-complex-based photosensitizers that will lead to the creation of effective and long-lasting CO2 reduction systems.	[115]

OrgD = Organic sensitizer [4,4′-bis(diethoxyphosphorylmethyl)-2,2′-bipyridine], MnP = Manganese complex, ReC = Re(4,4′-Y_2-bpy)$(CO)_3Cl$ (ReC = ReP; Y = $CH_2PO_3H_2$) and CBM: Conduction band

Very recently, conscious efforts have been made to explore the possibility of two semiconductors Z-scheme two-step photoexcitation approach to reduce CO_2 using water as the electron source in a powder-based suspension system or without sacrificial reagent. For example, Huang et al. [116] successfully developed a typical type II heterojunction utilizing composite materials made of In_2S_3/TiO_2. They discovered that a high separation efficiency of the photogenerated electron-hole pairs has been attained by adjusting the In_2S_3/TiO_2 ratio. Without the use of an extra sacrificial agent, it was found that 5 % In_2S_3/TiO_2 demonstrated a CH_4 generation rate of 16.21 $\mu mol\, g^{-1}\, h^{-1}$, and the catalytic activity is significantly higher than that of pure TiO_2 nanosheets. The large specific surface area and improved visible light harvesting of the hybrid catalyst were both credited with its high catalytic activity. In another study, Che and co-workers [117] demonstrated that Z-scheme g-C_3N_4/Ag_2CrO_4 photocatalysts exhibited excellent hydrogen evolution efficiency in comparison with the individual Ag_2CrO_4 and g-C_3N_4 under visible light irradiation (420 nm). They found that by optimizing the In_2S_3/TiO_2 ratio, a high separation was achieved. The composite that had the best mass-to-volume ratio, 23.1%, had the highest photocatalytic activity, which was 902.1 $\mu mol\, g^{-1}\, h^{-1}$. The creation of the Z-scheme g-C_3N_4/Ag_2CrO_4 heterostructures, which had greater separation and transfer efficiencies of the photogenerated electron-hole pairs, is credited with the increased photocatalytic activity. Additionally, the photocorrosion of Ag_2CrO_4 nanoparticles was significantly reduced due to the firm coupling of Ag_2CrO_4 and g-C_3N_4 in heterostructures. This research may bring fresh insights into the design of Z-scheme heterostructures and contribute to our understanding of the mechanism of g-C_3N_4/silver composites. In a related study, Sun et al. [118] reported type II heterostructure of In_2O_3/BiOI spherical nanosheets as a promising photocatalyst for the reduction of CO_2. The group found that the improved BI-10 had the highest photocatalytic yields, with CO and CH_4 yields of 11.98 mol g1h1 and 5.69 mol g1h1, respectively. As well as being 5.3 and 4.2 times higher than pure BiOI and pure In_2O_3 and 2.1 and 1.9 times higher than pure BiOI and pure In_2O_3, respectively, the yields of CO and CH_4 were also greater. This is explained by the type II heterojunction formed by the close contact of In_2O_3 and BiOI, which broadens the photoreaction's spectral

range and facilitates effective charge separation and transfer at the heterojunction interface. This research can serve as a model for catalyst modification that is generally applicable to photocatalysis.

A shuttle redox mediator was discovered to promote electron transfer between two semiconductors in these systems. Because of its numerous advantages, the semiconductor-based Z-scheme approach has become a popular candidate in photocatalytic CO_2 reduction research, but especially in water splitting. These include the ability to separate reduction/oxidation products as well as the use of a broader range of visible light. Furthermore, semiconductors with a reduction potential suitable for either CO_2 reduction or water oxidation can be used on each side of the system.

However, difficulties with thermodynamics, charge-transfer dynamics, applicability and practical synthesis are faced by all types of Z-scheme heterojunction. In this case, it is preferable to substitute Z-scheme in favour of a fresh idea that explicitly explains the mechanism of the photocatalytic CO_2 reduction reaction (PCRR).

8. S-scheme

To overcome the limitations of the Z-scheme heterojunctions, Yu and his colleagues [119] proposed a new step-scheme abbreviated as S-scheme heterojunction. This S-scheme heterojunction is made up of staggered band structures of reduction photocatalyst (RP) and oxidation photocatalyst (OP) which is similar to type II heterojunctions but with an absolutely different pathway of charge transfer. Unlike other types of heterojunctions, the RP of S-scheme photocatalyst is constructed with higher CB and VB levels and smaller work function compared to OP (**Figure 8a**). According to the review paper of Xu et al. [120] , the charge transfer pathway of S-scheme heterojunction can be explained in three steps as thus; (1) When OP and RP interact, electrons in the RP randomly disperse to OP, resulting in layer depletion and layer accumulation close to the interface in RP and OP, as shown in **Figure 8a**. The OP becomes more negatively charged, while the RP becomes more positively charged, and an internal electric field directing from the RP to the OP is formed at the same time (**Figure 8b)**. This internal electric field accelerates the transfer of photogenerated electrons from OP to RP (2) When the two semiconductors touch, their Fermi energy levels align to the same level, which causes an increase and decrease, respectively, in the Fermi levels of OP and RP (**Figure 8c**). (3) Due to the Coulombic attraction

between the holes and electrons, the photogenerated e^- in the CB of the OP and the h^+ in the VB of the RP are inclined at the interface. In summary, electron recombination in the CB of OP and hole recombination in the VB of RP are driven by three factors including the internal electric field, band bending and Coulombic attraction. Therefore, the powerful photogenerated electrons in the CB of RP and the holes in the VB of OP are preserved to take part in the PCRR while the useless electrons and holes are eliminated via recombination. It is important to note that the S-scheme heterojunction is suitable for PCRR because the reserved photogenerated electrons and holes are spatially separated and have significant redox abilities because of the diversified charge-transfer mode.

Considering the dynamic and unambiguous charge transfer mechanism, strong redox ability and accelerate electrons and holes of S-scheme heterojunction, researchers have developed strong interest particularly for PCRR. For instance, Zhang et al. [121] reported a novel S-scheme composite consisting of ultrasmall copper phosphosulfide (us-$Cu_3P|S$) nanocrystals anchored on 2D g-C3N4 nanosheets synthesized via a wet chemical method. The estimated work function (ϕ) of g-C_3N_4 and us-Cu_3PIS are 3.93 and 5.16 eV. The group claims that the Fermi levels of g-C3N4 and us$Cu_3P|S$ shift to the same energy level of 0.52 V when they are coupled, adjusting the band positions of the us-$Cu_3P|S$/CN composite (**Figure 9**). Such band alignment of g-C_3N_4 and us-$Cu_3P|S$ permits either type-II heterojunction or S-scheme interfaces, leading to two distinct electron transfer pathways. According to the S-scheme mechanism, it is possible that g-C_3N_4 conducts the H_2O oxidation reaction while us-$Cu_3P|S$ conducts the CO_2 reduction reaction because the VB position of us-$Cu_3P|S$ in the composite is below the O_2/H_2O standard redox potential. In a nutshell, us-Cu3P|S and g-C_3N_4 interact to form an S-scheme heterojunction that serves as an electron transfer channel and promotes the separation and migration of photogenerated charge carriers by forming interfacial P-N chemical bonds. As a result of the altered band structures of us-$Cu_3P|S$ and g-C_3N_4 during composite formation, a photocatalytic CO generation rate of 137 μmol g^{-1} h^{-1} which is eight times higher than that of pristine g-C_3N_4 is produced.

Aside from the previously mentioned 2D architecture g-C_3N_4, Wang and his colleagues [122] carefully encapsulated $ZnIn_2S_4$ nanosheets on the outer layer of TiO_2 hollow spheres in order to create a 1D hierarchical S-scheme $TiO_2@ZnIn_2S_4$ heterojunction for improved PCRR. The in situ irradiated x-ray photoelectron spectroscopy, electron

679 paramagnetic resonance and work function analysis demontrate S-scheme charge
680 transfer mechanism (**Figure 10)**. When compared to regular pristine $ZnIn_2S_4$ and TiO_2,
681 S-scheme TiO_2@$ZnIn_2S_4$ heterojunction photocatalyst performance is significantly
682 improved. S-scheme TiO_2@$ZnIn_2S_4$ heterojunction's total CO_2 photoreduction
683 conversion rates (the sum yield of CO, CH_3OH and CH_4) increased by 2.75 and 4.43
684 times, respectively. According to experimental results, this logical design offers a lot of
685 active sites and large surface areas for multi-electron PCRR as well as effectively
686 separating useful photogenerated electrons and holes.

687 In another recent study, a group of researchers [123] developed a novel S-scheme
688 heterojunction of $CsPbBr_3$ nanocrystals/CoAl layered double hydroxide nanosheets
689 composite as an efficient photocatalyst for CO_2 reduction (**Figure 11**). The S-scheme
690 heterojunction not only allowed photogenerated electron/hole pairs to separate, but it
691 also kept CB photoinduced reducing ability on the $CsPbBr_3$. Additionally, the increased
692 CO_2 adsorption and activation were significantly improved in the PCRR compared to
693 single photocatalyst. The CPB/LDH composite demonstrated significantly improved
694 photocatalytic properties in PCRR as a result of these synergistic actions. The 0.6
695 CPB/LDH sample had the highest activity, with quantum yield of 59.5 $mol.g^{-1}$ (CO +
696 CH_4) which were 9.9-fold higher than the original CoAl-LDH and 2.6-fold higher than
697 $CsPbBr_3$. Wang et al. recently reported hierarchical hollow structured S-scheme
698 photocatalysts of TiO_2 nanosheet arrays-decorated In_2O_3 hexagonal nanotubes by in-
699 situ hydrothermal method [124]. The team discovered that the In_2O_3@TiO_2
700 photocatalyst internal electric field acts as a powerful driving force for the S-scheme
701 electron transfer from the CB of TiO_2 to the VB of In_2O_3. For the selective
702 photocatalytic conversion of CO_2 with H_2O into hydrocarbon fuel (CH_4) without the
703 use of a sacrificial agent, the In_2O_3@TiO_2 catalysts demonstrated outstanding
704 performance. The S-scheme with the highest selectivity (88.1%) and yield (11.1 mol $g^{-1}h^{-1}$)
705 of the CH_4 product is In_2O_3@TiO_2-10 among all the tested photocatalysts.

706

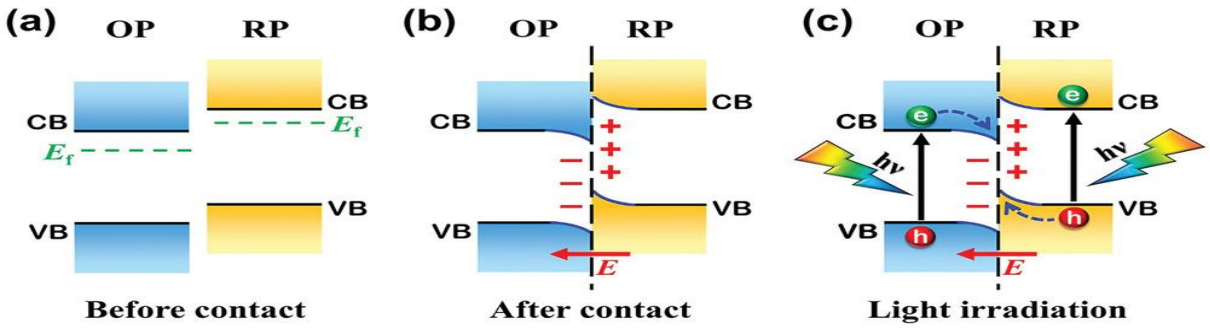

Figure 8: Mechanism of charge tranfer in S-scheme heterojunction. Adapted with the permision from ref. [125]. Copyright (2022) Willey Online Library.

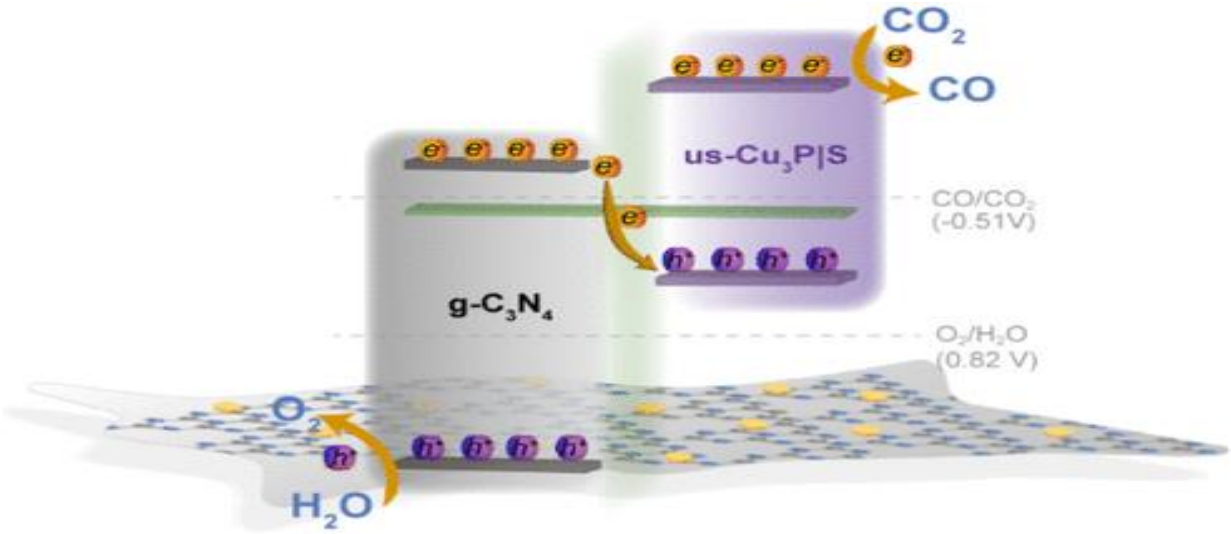

Figure 9: Charge tranfer route of us-Cu_3P|S/CN S-scheme heterojunction under irradiation. Adapted with the permision from ref.[121]. Copyright (2021) American Chemical Society

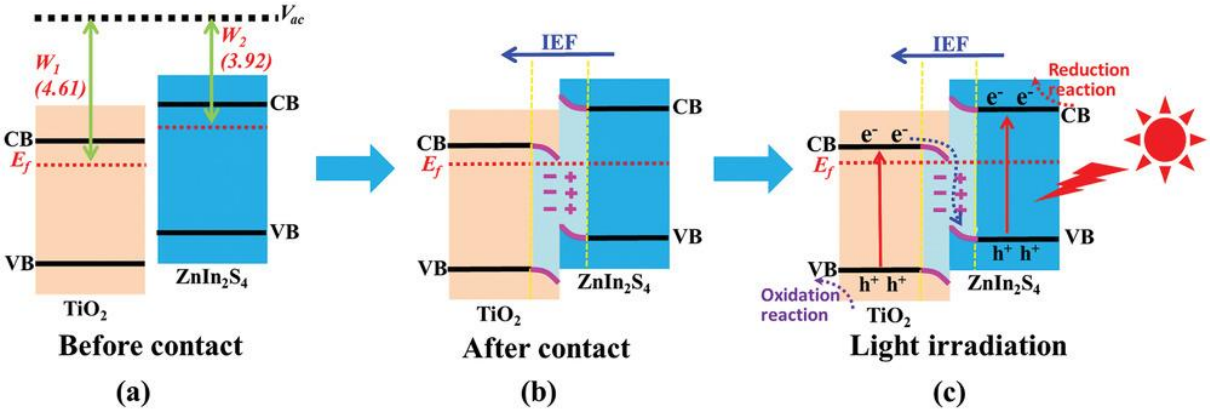

Figure 11: Charge tranfer mechanism of hierarchical S-scheme TiO_2@$ZnIn_2S_4$ heterojunction. Adapted with the permision from ref. [122]. Copyright (2021) Willey Online Library

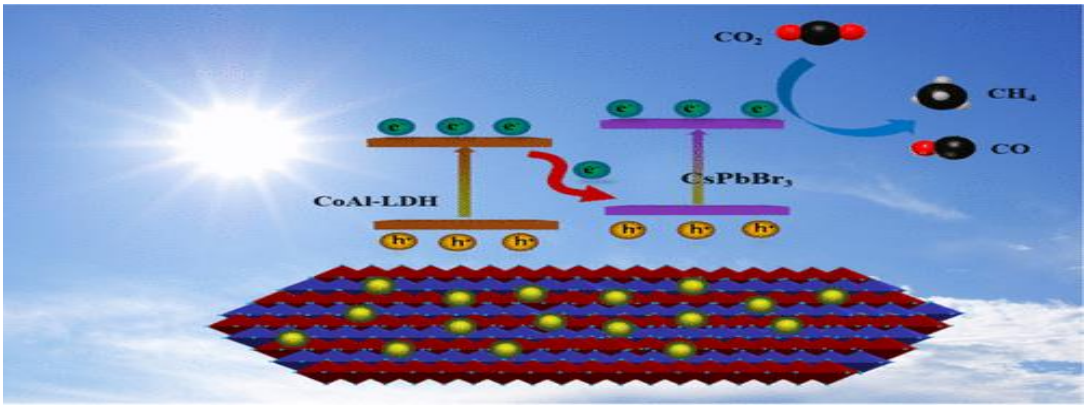

Figure 11: Mechanism of PCRR by CPB/LDH S-scheme heterojunction under irradiation. Adapted with the permision from ref.[123]. Copyright (2022) American Chemical Society

9. Organic photocatalysts

Without a brief overview of recent studies using microbes or organic materials as effective photocatalysts for CO_2 reduction, this review exercise would not have been completed. Photosynthetic biohybrid systems, which combine the remarkable light-harvesting abilities of semiconductors with the capacity for biological cells to synthesize energy, have become a promising platform for solar-to-chemical conversion. In recent time, Gai and co-authors [126] invented a non-photosynthetic bacteria called Moorella thermoacetica that efficiently reduces CO_2 to create acetic acid through an organic, π-conjugated semiconductor–bacteria biohybrid photosynthetic system (see **Figure 12**). In order to form a p-n heterojunction (PFP/PDI layer), which offers a higher hole/electron separation efficiency, both cationic electron-transporting (n-type) perylene diimide derivative (PDI) and hole-transporting (p-type) poly(fluorene-co-phenylene) (PFP) molecules were coated on the surface of the bacteria as photosensitizers. The cationic side chains of organic semiconductors might intercalate into cell membranes, assuring the effective electron transmission to bacteria. Additionally, the π-conjugated semiconductors have high light-harvesting capacity and biocompatibility. Moorella thermoacetica is able to utilize photoexcited electrons from the PFP/PDI heterojunction in order to activate the Wood-Ljungdahl pathway to produce acetic acid from CO_2 in the presence of light. This organic biohybrid's efficiency of 1.6% is comparable to that of previously reported inorganic biohybrid systems. In addition to opening up a new area for research into organic semiconductor applications in bioenergy, this work also offers a practical biomanufacturing method for

creating organic semiconductor–bacteria biohybrids for effective solar–to–chemical conversion.

Figure 12. Organic semiconductor-bacteria biohybrid photosynthetic pathway [126]

10. Conclusions and future outlook

Metal-organic frameworks, metal complexes, semiconductors, Z-schemes and organic photocatalysts designed for the reduction of CO_2 under visible light irradiation are reviewed. Furthermore, in order to produce a balance report, the review surveys computational studies on some of the aforementioned material. According to the literature, certain metal-organic frameworks, metal complexes, and semiconductors can function as suitable photocatalysts for CO_2 reduction with high selectivity and superior turnover number, producing desired products such as CO, CH_4, CH_3OH, HCOOH or $HCOO^-$. Overall, the findings demonstrate that metal-complex photocatalysts are most effective when immobilized on a semiconductor with a sufficiently negative conduction-band potential. Weaker electron donors that cannot be oxidized by the metal complex can be used as a result of this immobilization. Therefore, these metal complex/semiconductor hybrid photocatalysts outperform equivalent single-component systems having only a metal complex or a semiconductor under the identical reaction circumstances. The same outstanding synergistic effect was also reported for Z-scheme, MOFs and organic composites though with some unresolved challenges of charge transfer particularly with Z-scheme photocatalysts. As a prove of concept, S-scheme heterostructures was reported as a better replacement because of its unambiguous charge transfer mechanism. In addition, the review demonstrates the role of

functionalizing different photocatalysts platforms with co-catalyst for effective CO_2 adsorption, suppression of photogenerated electron-hole pairs, efficient light absorption etc. The literature also emphasizes the importance of theoretical investigations that can, at least partially, explain the electron-transfer process that takes place in such composites or hybrid systems, offering a logical strategy for future performance enhancements based on the optimization of MOFs, metal complexes, semiconductors and their hybrids.

Despite the success recorded so far in the field of photocatalytic CO_2 conversion to solar fuel production using metal complex, metal oxides, Z-scheme, organic semiconductors and MOFs, there is still a long way to go before having the scientific and technological capability to make this "artificial photosynthesis" practical to use for the production of hydrocarbon fuels and feedstock chemicals in large scale because of the unsatisfactory light harvesting, low-conversion efficiency, and lack of specific product selectivity. To begin with, developing more active and selective photocatalysts capable of successfully retarding charge recombination and capturing the solar spectrum is critical in the field of CO_2 photoreduction.

Another significant challenge in the field of CO_2 photoreduction is the lack of a standard technique for measuring photocatalytic performance, as well as a relevant parameter that allows quantitative comparison of CO_2 conversion efficiencies to specific fuels. One of the reasons is that the final activity and selectivity of CO_2 conversion are influenced by a variety of conditions such as light intensity and spectrum, reaction temperature, humidity, CO_2 concentration, pH and components of the photoreaction solution, mass and distribution of photocatalysts, and even reaction vessel shape. To correct this shortcoming and offer a solid foundation for further CO_2 conversion development, suitable performance evaluation systems for photocatalytic CO_2 conversion are required. A major issue that should not be overlooked in this field is confirming that CO_2 is the actual substrate for carbon-containing compounds, as state-of-the-art CO_2 photoreduction activities are currently quite low. One way to address this problem is to conduct trace experiments in order to confirm the carbon source.

Ultimately, a better understanding of photocatalytic CO_2 conversion reaction and deactivation mechanisms is required for optimizing surface, facets, phases, and other

material qualities, reaction circumstances, and other previously unknown features. It is general knowledge in the scientific community that photocatalytic CO_2 conversions to solar fuels are typically complex multielectron processes aided by H_2O, and the activity and selectivity of specific products compete with those of other products. A combination of experimental and theoretical findings from fundamental investigations and computer simulations should be favored since it is the most effective way to increase our understanding of CO_2 photoreduction mechanisms. In summary, photocatalytic CO_2 conversion to solar fuels is a technology that meets two goals with one method, providing a package solution to present global warming and energy demand by utilizing unlimited solar energy and increasing atmospheric CO_2. As a result, in both theory and practice, the research and design of CO_2 photoreduction systems with high stability, recyclability, nontoxicity, high efficiency, and wide spectral response under sunlight irradiation is crucial. It is our hope that this review work will channel a new path and concomitantly play an interesting role in this important research field.

Funding

This research received no external funding

Acknowledgements

Alli, Y.A. would like to appreciate LCC-CNRS and Prof. Karine Philippot in particular for providing him with laboratory space and enabling environment for postdoctoral research activities

Conflicts of interest

The authors declare no conflict of interest

References

[1] Liang S, Zeng G, Zhong X, Deng H, Zhong Z, Lin Z, et al. Efficient photoreduction of diluted CO2 using lattice-strained Ni1− xSe nanoflowers. Journal of CO2 Utilization 2022;64:102193.

[2] Saini S, Abraham BM, Jain SL. Light assisted nickel (II) grafted-g-carbon nitride molecular hybrid promoted hydrocarboxylation of olefins with CO2 at atmospheric pressure condition. Journal of CO2 Utilization 2022;55:101812.

[3] Perini JAL, Torquato LDM, Irikura K, Zanoni MVB. Ag/polydopamine-modified Ti/TiO2 nanotube arrays: A platform for enhanced CO2 photoelectroreduction to methanol. Journal of CO2 Utilization 2019;34:596–605.

[4] Chair K, Luna Caceres CA, Rajak S, Schott O, Ramírez-Caballero GE, Maris T, et al. Photocatalytic Carbon Dioxide Reduction and Density Functional Theory Investigation of 2, 6-(Pyridin-2-yl)-1, 3, 5-triazine-2, 4-diamine and Its Cobalt and Nickel Complexes. ACS Appl Energy Mater 2022.

[5] Chan B, Gill PMW, Kimura M. Assessment of DFT Methods for Transition Metals with the TMC151 Compilation of Data Sets and Comparison with Accuracies for Main-Group Chemistry. J Chem Theory Comput 2019;15:acs.jctc.9b00239. https://doi.org/10.1021/acs.jctc.9b00239.

[6] Pinter B, Chankisjijev A, Geerlings P, Harvey JN. Conceptual Insights into DFT Spin-State Energetics of Octahedral Transition-Metal Complexes through a Density Difference Analysis. Chemistry - A European Journal 2018;24:5281–92. https://doi.org/10.1002/chem.201704657.

[7] Bühl M, Reimann C, Pantazis DA, Bredow T, Neese F. Geometries of third-row transition-metal complexes from density-functional theory. J Chem Theory Comput 2008;4:1449–59. https://doi.org/10.1021/ct800172j.

[8] Castro-Ocampo O, Celaya CA, González-Reyes L, Hernández-Pérez I, Garibay-Febles V, Jaramillo-Quintero OA, et al. Understanding hydroxyl radicals addition to CO2 on α-Fe2O3(1 1 0) surface photocatalyst for organic compounds production. Fuel 2022;310. https://doi.org/10.1016/j.fuel.2021.122465.

[9] Zhou Z, Liu Y, Li M, Gu JD. Two or three domains: a new view of tree of life in the genomics era. Appl Microbiol Biotechnol 2018;102:3049–58. https://doi.org/10.1007/s00253-018-8831-x.

[10] Laun J, Bredow T. BSSE-corrected consistent Gaussian basis sets of triple-zeta valence with polarization quality of the sixth period for solid-state calculations. J Comput Chem 2021;42:1064–72.

[11] Onawole AT, Hussein IA, Saad MA, Ismail N, Alshami A, Nasser MS. Theoretical Studies of a Silica Functionalized Acrylamide for Calcium Scale Inhibition. Polymers (Basel) 2022;14:2073–4360.

[12] Zhou J, Li J, Kan L, Zhang L, Huang Q, Yan Y, et al. Linking oxidative and reductive clusters to prepare crystalline porous catalysts for photocatalytic CO2 reduction with H2O. Nat Commun 2022;13:1–10. https://doi.org/10.1038/s41467-022-32449-z.

[13] Yin Q, Alexandrov E V., Si D, Huang Q, Fang Z, Zhang Y, et al. Metallization-Prompted Robust Porphyrin-Based Hydrogen-Bonded Organic Frameworks for

Photocatalytic CO 2 Reduction . Angewandte Chemie 2022;134. https://doi.org/10.1002/ange.202115854.

[14] De La Torre P, Derrick JS, Snider A, Smith PT, Loipersberger M, Head-Gordon M, et al. Exchange Coupling Determines Metal-Dependent Efficiency for Iron- and Cobalt-Catalyzed Photochemical CO2 Reduction. ACS Catal 2022;12:8484–93. https://doi.org/10.1021/acscatal.2c02072.

[15] Abdelhamid HN. Removal of carbon dioxide using zeolitic imidazolate frameworks: Adsorption and conversion via catalysis. Appl Organomet Chem 2022;36:1–38. https://doi.org/10.1002/aoc.6753.

[16] Zeng JY, Wang XS, Xie BR, Li QR, Zhang XZ. Large π-Conjugated Metal-Organic Frameworks for Infrared-Light-Driven CO2Reduction. J Am Chem Soc 2022;144:1218–31. https://doi.org/10.1021/jacs.1c10110.

[17] Li S, Zhang Y, Hu Y, Wang B, Sun S, Yang X, et al. Predicting metal-organic frameworks as catalysts to fix carbon dioxide to cyclic carbonate by machine learning. Journal of Materiomics 2021;7:1029–38. https://doi.org/10.1016/j.jmat.2021.02.005.

[18] Halmann M. Photoelectrochemical reduction of aqueous carbon dioxide on p-type gallium phosphide in liquid junction solar cells. Nature 1978;275:115–6.

[19] Khalil M, Gunlazuardi J, Ivandini TA, Umar A. Photocatalytic conversion of CO2 using earth-abundant catalysts: A review on mechanism and catalytic performance. Renewable and Sustainable Energy Reviews 2019;113. https://doi.org/10.1016/j.rser.2019.109246.

[20] Li K, An X, Park KH, Khraisheh M, Tang J. A critical review of CO2 photoconversion: Catalysts and reactors. Catal Today 2014;224:3–12. https://doi.org/10.1016/j.cattod.2013.12.006.

[21] Fan W, Zhang Q, Wang Y. Semiconductor-based nanocomposites for photocatalytic H2 production and CO2 conversion. Physical Chemistry Chemical Physics 2013;15:2632–49. https://doi.org/10.1039/c2cp43524a.

[22] Sun Z, Dong J, Chen C, Zhang S, Zhu Y. Photocatalytic and electrocatalytic CO2 conversion: from fundamental principles to design of catalysts. Journal of Chemical Technology and Biotechnology 2021;96:1161–75. https://doi.org/10.1002/jctb.6653.

[23] Kuramochi Y, Ishitani O, Ishida H. Reaction mechanisms of catalytic photochemical CO2 reduction using Re(I) and Ru(II) complexes. Coord Chem Rev 2018;373:333–56. https://doi.org/10.1016/j.ccr.2017.11.023.

[24] Ohtani B. Revisiting the fundamental physical chemistry in heterogeneous photocatalysis: Its thermodynamics and kinetics. Physical Chemistry Chemical Physics 2014;16:1788–97. https://doi.org/10.1039/c3cp53653j.

[25] Zürch M, Chang HT, Borja LJ, Kraus PM, Cushing SK, Gandman A, et al. Direct and simultaneous observation of ultrafast electron and hole dynamics in germanium. Nat Commun 2017;8. https://doi.org/10.1038/ncomms15734.

[26] Shehzad N, Tahir M, Johari K, Murugesan T, Hussain M. A critical review on TiO2 based photocatalytic CO2 reduction system: Strategies to improve efficiency. Journal of CO2 Utilization 2018;26:98–122. https://doi.org/10.1016/j.jcou.2018.04.026.

[27] Maeda K. Metal-Complex/Semiconductor Hybrid Photocatalysts and Photoelectrodes for CO2 Reduction Driven by Visible Light. Advanced Materials 2019;31. https://doi.org/10.1002/adma.201808205.

[28] Hawecker J, Lehn J -M, Ziessel R. Photochemical and Electrochemical Reduction of Carbon Dioxide to Carbon Monoxide Mediated by (2,2′-Bipyridine)tricarbonylchlororhenium(I) and Related Complexes as Homogeneous Catalysts. Helv Chim Acta 1986;69:1990–2012. https://doi.org/10.1002/hlca.19860690824.

[29] Kumagai H, Tamaki Y, Ishitani O. Photocatalytic Systems for CO2 Reduction: Metal-Complex Photocatalysts and Their Hybrids with Photofunctional Solid Materials. Acc Chem Res 2022;55:978–90. https://doi.org/10.1021/acs.accounts.1c00705.

[30] Takeda H, Kamiyama H, Okamoto K, Irimajiri M, Mizutani T, Koike K, et al. Highly Efficient and Robust Photocatalytic Systems for CO2 Reduction Consisting of a Cu(I) Photosensitizer and Mn(I) Catalysts. J Am Chem Soc 2018;140:17241–54. https://doi.org/10.1021/jacs.8b10619.

[31] Fujishima A, Honda K. Electrochemical photolysis of water at a semiconductor electrode. Nature 1972;238:37–8. https://doi.org/10.1038/238037a0.

[32] Sharma A, Hosseini-Bandegharaei A, Kumar N, Kumar S, Kumari K. Insight into ZnO/carbon hybrid materials for photocatalytic reduction of CO2: An in-depth review. Journal of CO2 Utilization 2022;65. https://doi.org/10.1016/j.jcou.2022.102205.

[33] Kim J, Kwon EE. Photoconversion of carbon dioxide into fuels using semiconductors. Journal of CO2 Utilization 2019;33:72–82. https://doi.org/10.1016/J.JCOU.2019.05.012.

[34] Yoshino S, Takayama T, Yamaguchi Y, Iwase A, Kudo A. CO2Reduction Using Water as an Electron Donor over Heterogeneous Photocatalysts Aiming at

Artificial Photosynthesis. Acc Chem Res 2022;55:966–77. https://doi.org/10.1021/acs.accounts.1c00676.

[35] Fall B, Gaye C, Niang M, Alli YA, Diaw AKD, Fall M, et al. Removal of Toxic Chromium Ions in Aqueous Medium Using a New Sorbent Based on rGO@CNT@Fe2O3. Chemistry Africa 2022. https://doi.org/10.1007/s42250-022-00499-x.

[36] Guo Q, Xu J, Luo Y, Yang Y, Wang Z, He H. Cocatalyst Modification of AgTaO3 Photocatalyst for Conversion of Carbon Dioxide with Water. The Journal of Physical Chemistry C 2021;125:26389–97. https://doi.org/10.1021/acs.jpcc.1c06502.

[37] Liu J, Liu M, Yang X, Chen H, Frank Liu S, Yan J. Photo-Redeposition Synthesis of Bimetal Pt–Cu Co-catalysts for TiO2 Photocatalytic Solar-Fuel Production. ACS Sustainable Chemistry & Engineering 2020;8:6055–64. https://doi.org/10.1021/acssuschemeng.0c00969.

[38] Shen J, Wu Z, Li C, Zhang C, Genest A, Rupprechter G, et al. Emerging applications of MXene materials in CO2 photocatalysis. FlatChem 2021;28. https://doi.org/10.1016/j.flatc.2021.100252.

[39] Zhang X, Zhang Z, Li J, Zhao X, Wu D, Zhou Z. Ti2CO2 MXene: A highly active and selective photocatalyst for CO2 reduction. J Mater Chem A Mater 2017;5:12899–903. https://doi.org/10.1039/c7ta03557h.

[40] Li Y, Zhang M, Liu Y, Zhao Q, Li X, Zhou Q, et al. Construction of Bronze TiO2/Ti3 C2 MXene/Ag3 PO4 Ternary Composite Photocatalyst toward High Photocatalytic Performance. Catalysts 2022;12. https://doi.org/10.3390/catal12060599.

[41] Pal K, Sajjadifar S, Abd Elkodous M, Alli YA, Gomes F, Jeevanandam J, et al. Soft, Self-Assembly Liquid Crystalline Nanocomposite for Superior Switching. Electronic Materials Letters 2019;15:84–101. https://doi.org/10.1007/s13391-018-0098-y.

[42] Singh P, Srivastava R. Utilization of bio-inspired catalyst for CO2 reduction into green fuels: Recent advancement and future perspectives. Journal of CO2 Utilization 2021;53. https://doi.org/10.1016/j.jcou.2021.101748.

[43] W. White D, Esckilsen D, Kyu Lee S, W. Ragsdale S, Brian Dyer R. Efficient, Light-Driven Reduction of CO2 to CO by a Carbon Monoxide Dehydrogenase–CdSe/CdS Nanorod Photosystem. J Phys Chem Lett 2022;13:5553–6. https://doi.org/10.1021/acs.jpclett.2c01412.

[44] Bétard A, Fischer RA. Metal-organic framework thin films: From fundamentals to applications. Chem Rev 2012;112:1055–83. https://doi.org/10.1021/cr200167v.

[45] Kitagawa S, Kitaura R, Noro SI. Functional porous coordination polymers. Angewandte Chemie - International Edition 2004;43:2334–75. https://doi.org/10.1002/anie.200300610.

[46] Liu G, Sheng Y, Ager JW, Kraft M, Xu R. Research advances towards large-scale solar hydrogen production from water. EnergyChem 2019;1:100014. https://doi.org/10.1016/j.enchem.2019.100014.

[47] Oladoye PO, Adegboyega SA, Giwa A-RA. Remediation potentials of composite metal-organic frameworks (MOFs) for dyes as water contaminants: A comprehensive review of recent literatures. Environ Nanotechnol Monit Manag 2021;16:100568. https://doi.org/10.1016/j.enmm.2021.100568.

[48] Elhenawy SEM, Khraisheh M, Almomani F, Walker G. Metal-organic frameworks as a platform for CO2 capture and chemical processes: Adsorption, membrane separation, catalytic-conversion, and electrochemical reduction of CO2. Catalysts 2020;10:1–33. https://doi.org/10.3390/catal10111293.

[49] Yan A, Shi X, Huang F, Fujitsuka M, Majima T. Efficient photocatalytic H2 evolution using NiS/ZnIn2S4 heterostructures with enhanced charge separation and interfacial charge transfer. Appl Catal B 2019;250:163–70. https://doi.org/10.1016/j.apcatb.2019.02.075.

[50] Corma A, García H, Llabrés I Xamena FX. Engineering metal organic frameworks for heterogeneous catalysis. Chem Rev 2010;110:4606–55. https://doi.org/10.1021/cr9003924.

[51] Pannwitz A, Wenger OS. Proton-coupled multi-electron transfer and its relevance for artificial photosynthesis and photoredox catalysis. Chemical Communications 2019;55:4004–14. https://doi.org/10.1039/c9cc00821g.

[52] Ejeromedoghene O, Oderinde O, Okoye CO, Oladipo A, Alli YA. Microporous metal-organic frameworks based on deep eutectic solvents for adsorption of toxic gases and volatile organic compounds: A review. Chemical Engineering Journal Advances 2022;12. https://doi.org/10.1016/j.ceja.2022.100361.

[53] Hwang A, Bhan A. Deactivation of Zeolites and Zeotypes in Methanol-to-Hydrocarbons Catalysis: Mechanisms and Circumvention. Acc Chem Res 2019:2647–56. https://doi.org/10.1021/acs.accounts.9b00204.

[54] Choudhary A, Das B, Ray S. Encapsulated Schiff base nickel complex in zeolite Y: Correlation between catalytic activities and extent of distortion supported by

experimental and DFT studies. Inorganica Chim Acta 2017;462:256–65. https://doi.org/10.1016/j.ica.2017.04.003.

[55] Li S, Yang H, Wang S, Wang J, Fan W, Dong M. Improvement of adsorption and catalytic properties of zeolites by precisely controlling their particle morphology. Chemical Communications 2022;58:2041–54. https://doi.org/10.1039/d1cc05537b.

[56] Algieri C, Drioli E. Zeolite membranes: Synthesis and applications. Sep Purif Technol 2022;278. https://doi.org/10.1016/j.seppur.2021.119295.

[57] Madhu J, Ramakrishnan VM, Santhanam A, Natarajan M, Palanisamy B, Velauthapillai D, et al. Comparison of three different structures of zeolites prepared by template-free hydrothermal method and its CO2 adsorption properties. Environ Res 2022:113949. https://doi.org/10.1016/j.envres.2022.113949.

[58] Kubička D, Kikhtyanin O. Opportunities for zeolites in biomass upgrading-Lessons from the refining and petrochemical industry. Catal Today 2015;243:10–22. https://doi.org/10.1016/j.cattod.2014.07.043.

[59] Ennaert T, van Aelst J, Dijkmans J, de Clercq R, Schutyser W, Dusselier M, et al. Potential and challenges of zeolite chemistry in the catalytic conversion of biomass. Chem Soc Rev 2016;45:584–611. https://doi.org/10.1039/c5cs00859j.

[60] Allendorf MD, Schwartzberg A, Stavila V, Talin AA. A roadmap to implementing metal-organic frameworks in electronic devices: Challenges and critical directions. Chemistry - A European Journal 2011;17:11372–88. https://doi.org/10.1002/chem.201101595.

[61] Usman M. Concatenated convolution-polar codes over Rayleigh channels degraded as erasure channels. Proceedings of the 10th International Conference on Intelligent Systems and Control, ISCO 2016, Institute of Electrical and Electronics Engineers Inc.; 2016. https://doi.org/10.1109/ISCO.2016.7727053.

[62] Wang D, Li Z. Iron-based metal–organic frameworks (MOFs) for visible-light-induced photocatalysis. Research on Chemical Intermediates 2017;43:5169–86. https://doi.org/10.1007/s11164-017-3042-0.

[63] Zhang T, Lin W. Metal-organic frameworks for artificial photosynthesis and photocatalysis. Chem Soc Rev 2014;43:5982–93. https://doi.org/10.1039/c4cs00103f.

[64] Ezugwu CI, Liu S, Li C, Zhuiykov S, Roy S, Verpoort F. Engineering metal-organic frameworks for efficient photocatalytic conversion of CO2 into solar fuels. Coord Chem Rev 2022;450. https://doi.org/10.1016/j.ccr.2021.214245.

[65] Alvaro M, Carbonell E, Ferrer B, Llabrés I Xamena FX, Garcia H. Semiconductor behavior of a metal-organic framework (MOF). Chemistry - A European Journal 2007;13:5106–12. https://doi.org/10.1002/chem.200601003.

[66] Gordillo MA, Benavides PA, Panda DK, Saha S. The Advent of Electrically Conducting Double-Helical Metal-Organic Frameworks Featuring Butterfly-Shaped Electron-Rich π-Extended Tetrathiafulvalene Ligands. ACS Appl Mater Interfaces 2020;12:12955–61. https://doi.org/10.1021/acsami.9b20234.

[67] Lu J, Wang SH, Li Y, Wang WF, Sun C, Li PX, et al. Heat-resistant Pb(ii)-based X-ray scintillating metal-organic frameworks for sensitive dosage detectionviaan aggregation-induced luminescent chromophore. Dalton Transactions 2020;49:7309–14. https://doi.org/10.1039/d0dt00974a.

[68] Ludig S, Haller M, Bauer N. Tackling long-term climate change together: The case of flexible CCS and fluctuating renewable energy. Energy Procedia, vol. 4, Elsevier Ltd; 2011, p. 2580–7. https://doi.org/10.1016/j.egypro.2011.02.156.

[69] Miyagawa T, Matsuhashi R, Murai S, Muraok M. Comparative assessment of CCS with other technologies mitigating climate change. Energy Procedia, vol. 4, Elsevier Ltd; 2011, p. 5710–4. https://doi.org/10.1016/j.egypro.2011.02.565.

[70] Koljonen T, Flyktman M, Lehtilä A, Pahkala K, Peltola E, Savolainen I. The role of CCS and renewables in tackling climate change. Energy Procedia, vol. 1, 2009, p. 4323–30. https://doi.org/10.1016/j.egypro.2009.02.245.

[71] Hanaoka T, Masui T. Exploring the 2 °c Target Scenarios by Considering Climate Benefits and Health Benefits - Role of Biomass and CCS. Energy Procedia, vol. 114, Elsevier Ltd; 2017, p. 2618–30. https://doi.org/10.1016/j.egypro.2017.03.1424.

[72] Flaig RW, Osborn Popp TM, Fracaroli AM, Kapustin EA, Kalmutzki MJ, Altamimi RM, et al. The Chemistry of CO2 Capture in an Amine-Functionalized Metal-Organic Framework under Dry and Humid Conditions. J Am Chem Soc 2017;139:12125–8. https://doi.org/10.1021/jacs.7b06382.

[73] Zou X;, Zhu G. CO2 Capture with MOF Membranes: In Microporous Materials for Separation Membranes. Hoboken, NJ, USA: John Wiley & Sons; 2019.

[74] Kang Z, Fan L, Sun D. Recent advances and challenges of metal-organic framework membranes for gas separation. J Mater Chem A Mater 2017;5:10073–91. https://doi.org/10.1039/c7ta01142c.

[75] Elhenawy SEM, Khraisheh M, Almomani F, Walker G. Metal-organic frameworks as a platform for CO2 capture and chemical processes: Adsorption, membrane separation, catalytic-conversion, and electrochemical reduction of CO2. Catalysts 2020;10:1–33. https://doi.org/10.3390/catal10111293.

[76] Xiang Z, Peng X, Cheng X, Li X, Cao D. CNT@Cu3(BTC)2 and metal-organic frameworks for separation of CO2/CH4 mixture. Journal of Physical Chemistry C 2011;115:19864–71. https://doi.org/10.1021/jp206959k.

[77] Li T, Sullivan JE, Rosi NL. Design and preparation of a core-shell metal-organic framework for selective CO2 capture. J Am Chem Soc 2013;135:9984–7. https://doi.org/10.1021/ja403008j.

[78] Qian D, Lei C, Hao GP, Li WC, Lu AH. Synthesis of hierarchical porous carbon monoliths with incorporated metal-organic frameworks for enhancing volumetric based CO2 capture capability. ACS Appl Mater Interfaces 2012;4:6125–32. https://doi.org/10.1021/am301772k.

[79] Hayashi H, Côté AP, Furukawa H, O'Keeffe M, Yaghi OM. Zeolite A imidazolate frameworks. Nat Mater 2007;6:501–6. https://doi.org/10.1038/nmat1927.

[80] Chen B, Ma S, Hurtado EJ, Lobkovsky EB, Zhou HC. A triply interpenetrated microporous metal-organic framework for selective sorption of gas molecules. Inorg Chem 2007;46:8490–2. https://doi.org/10.1021/ic7014034.

[81] Masoomi MY, Stylianou KC, Morsali A, Retailleau P, Maspoch D. Selective CO2 capture in metal-organic frameworks with azine-functionalized pores generated by mechanosynthesis. Cryst Growth Des 2014;14:2092–6. https://doi.org/10.1021/cg500033b.

[82] Ma S, Wang X sen, Manis ES, Collier CD, Zhou HC. Metal-organic framework based on a trinickel secondary building unit exhibiting gas-sorption hysteresis. Inorg Chem 2007;46:3432–4. https://doi.org/10.1021/ic070338v.

[83] Hong DH, Suh MP. Selective CO2adsorption in a metal–organic framework constructed from an organic ligand with flexible joints. Chemical Communications 2012;48:9168–70. https://doi.org/10.1039/c2cc34482c.

[84] Kitaura R, Seki K, Akiyama G, Kitagawa S. Flexible Coordination Polymers Porous Coordination-Polymer Crystals with Gated Channels Specific for Supercritical Gases**. Angew Chem Int Ed 2003;42:428–31.

[85] Maji TK, Matsuda R, Kitagawa S. A flexible interpenetrating coordination framework with a bimodal porous functionality. Nat Mater 2007;6:142–8. https://doi.org/10.1038/nmat1827.

[86] Lin Y, Yan Q, Kong C, Chen L. Polyethyleneimine incorporated metal-organic frameworks adsorbent for highly selective CO2 capture. Sci Rep 2013;3. https://doi.org/10.1038/srep01859.

[87] Bataille T, Bracco S, Comotti A, Costantino F, Guerri A, Ienco A, et al. Solvent dependent synthesis of micro-and nano-crystalline phosphinate based 1D tubular

MOF: Structure and CO2 adsorption selectivity. CrystEngComm 2012;14:7170–3. https://doi.org/10.1039/c2ce26138c.

[88] Llewellyn PL, Bourrelly S, Serre C, Filinchuk Y, Férey G. How hydration drastically improves adsorption selectivity for CO 2 over CH4 in the flexible chromium terephthalate MIL-53. Angewandte Chemie - International Edition 2006;45:7751–4. https://doi.org/10.1002/anie.200602278.

[89] Zheng B, Yun R, Bai J, Lu Z, Du L, Li Y. Expanded porous MOF-505 analogue exhibiting large hydrogen storage capacity and selective carbon dioxide adsorption. Inorg Chem 2013;52:2823–9. https://doi.org/10.1021/ic301598n.

[90] Chen B, Ma S, Zapata F, Fronczek FR, Lobkovsky EB, Zhou HC. Rationally designed micropores within a metal-organic framework for selective sorption of gas molecules. Inorg Chem 2007;46:1233–6. https://doi.org/10.1021/ic0616434.

[91] Adabala S, Dutta DP. A review on recent advances in metal chalcogenide-based photocatalysts for CO2reduction. J Environ Chem Eng 2022;10:107763. https://doi.org/10.1016/j.jece.2022.107763.

[92] Ezugwu CI, Liu S, Li C, Zhuiykov S, Roy S, Verpoort F. Engineering metal-organic frameworks for efficient photocatalytic conversion of CO2 into solar fuels. Coord Chem Rev 2022;450:214245. https://doi.org/10.1016/j.ccr.2021.214245.

[93] Toyao T, Saito M, Dohshi S, Mochizuki K, Iwata M, Higashimura H, et al. Development of a Ru complex-incorporated MOF photocatalyst for hydrogen production under visible-light irradiation. Chemical Communications 2014;50:6779–81. https://doi.org/10.1039/c4cc02397h.

[94] Deng X, Li Z, García H. Visible Light Induced Organic Transformations Using Metal-Organic-Frameworks (MOFs). Chemistry - A European Journal 2017;23:11189–209. https://doi.org/10.1002/chem.201701460.

[95] Al-Rowaili FN, Zahid U, Onaizi S, Khaled M, Jamal A, AL-Mutairi EM. A review for Metal-Organic Frameworks (MOFs) utilization in capture and conversion of carbon dioxide into valuable products. Journal of CO2 Utilization 2021;53:101715. https://doi.org/10.1016/j.jcou.2021.101715.

[96] Toyao T, Saito M, Dohshi S, Mochizuki K, Iwata M, Higashimura H, et al. Development of a Ru complex-incorporated MOF photocatalyst for hydrogen production under visible-light irradiation. Chemical Communications 2014;50:6779–81. https://doi.org/10.1039/c4cc02397h.

[97] Zhang Y, Liu H, Gao F, Tan X, Cai Y, Hu B, et al. Application of MOFs and COFs for photocatalysis in CO2 reduction, H2 generation, and environmental

treatment. EnergyChem 2022;4:100078. https://doi.org/10.1016/j.enchem.2022.100078.

[98] Alvaro M, Carbonell E, Ferrer B, Llabrés I Xamena FX, Garcia H. Semiconductor behavior of a metal-organic framework (MOF). Chemistry - A European Journal 2007;13:5106–12. https://doi.org/10.1002/chem.200601003.

[99] Ješić D, Lašič Jurković D, Pohar A, Suhadolnik L, Likozar B. Engineering photocatalytic and photoelectrocatalytic CO2 reduction reactions: Mechanisms, intrinsic kinetics, mass transfer resistances, reactors and multi-scale modelling simulations. Chemical Engineering Journal 2021;407. https://doi.org/10.1016/j.cej.2020.126799.

[100] Mu Q, Zhu W, Li X, Zhang C, Su Y, Lian Y, et al. Electrostatic charge transfer for boosting the photocatalytic CO2 reduction on metal centers of 2D MOF/rGO heterostructure. Appl Catal B 2020;262. https://doi.org/10.1016/j.apcatb.2019.118144.

[101] Omar S, Shkir M, Ajmal Khan M, Ahmad Z, AlFaify S. A comprehensive study on molecular geometry, optical, HOMO-LUMO, and nonlinear properties of 1,3-diphenyl-2-propen-1-ones chalcone and its derivatives for optoelectronic applications: A computational approach. Optik (Stuttg) 2020;204. https://doi.org/10.1016/j.ijleo.2020.164172.

[102] Ma S, Wang X sen, Manis ES, Collier CD, Zhou HC. Metal-organic framework based on a trinickel secondary building unit exhibiting gas-sorption hysteresis. Inorg Chem 2007;46:3432–4. https://doi.org/10.1021/ic070338v.

[103] Al-Rowaili FN, Zahid U, Onaizi S, Khaled M, Jamal A, AL-Mutairi EM. A review for Metal-Organic Frameworks (MOFs) utilization in capture and conversion of carbon dioxide into valuable products. Journal of CO2 Utilization 2021;53. https://doi.org/10.1016/j.jcou.2021.101715.

[104] Zhang W, Mohamed AR, Ong WJ. Z-Scheme Photocatalytic Systems for Carbon Dioxide Reduction: Where Are We Now? Angewandte Chemie - International Edition 2020;59:22894–915. https://doi.org/10.1002/anie.201914925.

[105] Xu Q, Zhang L, Yu J, Wageh S, Al-ghamdi AA, Jaroniec M. Direct Z-scheme photocatalysts : Principles , synthesis , and applications. Materials Today 2018;xxx. https://doi.org/10.1016/j.mattod.2018.04.008.

[106] Low J, Jiang C, Cheng B, Wageh S, Al-Ghamdi AA, Yu J. A Review of Direct Z-Scheme Photocatalysts. Small Methods 2017;1. https://doi.org/10.1002/smtd.201700080.

[107] Okoye-Chine CG, Otun K, Shiba N, Rashama C, Ugwu SN, Onyeaka H, et al. Conversion of carbon dioxide into fuels—A review. Journal of CO2 Utilization 2022;62:102099. https://doi.org/10.1016/J.JCOU.2022.102099.

[108] Sato S, Arai T, Morikawa T. Toward solar-driven photocatalytic CO2 reduction using water as an electron donor. Inorg Chem 2015;54:5105–13. https://doi.org/10.1021/ic502766g.

[109] Nakada A, Kuriki R, Sekizawa K, Nishioka S, Vequizo JJM, Uchiyama T, et al. Effects of Interfacial Electron Transfer in Metal Complex-Semiconductor Hybrid Photocatalysts on Z-Scheme CO2 Reduction under Visible Light. ACS Catal 2018;8:9744–54. https://doi.org/10.1021/acscatal.8b03062.

[110] Tsounis C, Kuriki R, Shibata K, Jhon M. Vequizo J, Lu D, Yamakata A, et al. Copolymerization Approach to Improving Ru(II)-Complex/C3N4 Hybrid Photocatalysts for Visible-Light CO2 Reduction. ACS Sustainable Chemistry & Engineering 2018;6:15333–40. https://doi.org/10.1021/acssuschemeng.8b03782.

[111] Shirai S, Sato S, M. Suzuki T, Jinnouchi R, Ohba N, Asahi R, et al. Effects of Ta2O5 Surface Modification by NH3 on the Electronic Structure of a Ru-Complex/N–Ta2O5 Hybrid Photocatalyst for Selective CO2 Reduction. The Journal of Physical Chemistry C 2018;122:1921–9. https://doi.org/10.1021/acs.jpcc.7b09670.

[112] Huang P, Pantovich SA, Okolie NO, Deskins NA, Li G. Hybrid Carbon Dioxide Reduction Photocatalysts Consisting of Macrocyclic Cobalt(III) Complexes Deposited on Semiconductor Surfaces. ChemPhotoChem 2020;4:420–6. https://doi.org/10.1002/cptc.201900282.

[113] Roy S, Reisner E. Visible-Light-Driven CO2 Reduction by Mesoporous Carbon Nitride Modified with Polymeric Cobalt Phthalocyanine. Angewandte Chemie - International Edition 2019;58:12180–4. https://doi.org/10.1002/anie.201907082.

[114] Woo S-J, Choi S, Kim S-Y, Soo Kim P, Hyoung Jo J, Hoon Kim C, et al. Highly Selective and Durable Photochemical CO2 Reduction by Molecular Mn(I) Catalyst Fixed on a Particular Dye-Sensitized TiO2 Platform. ACS Catal 2019;9:2580–93. https://doi.org/10.1021/acscatal.8b03816.

[115] Cheong H-Y, Kim S-Y, Cho Y-J, Won Cho D, Hoon Kim C, Son H-J, et al. Photosensitization Behavior of Ir(III) Complexes in Selective Reduction of CO2 by Re(I)-Complex-Anchored TiO2 Hybrid Catalyst. Inorg Chem 2017;56:12042–53. https://doi.org/10.1021/acs.inorgchem.7b01963.

[116] Huang G, Shen Q, Ma X, Zhong J, Chen J, Huang J, et al. Preparation of an In2S3/TiO2 Heterostructure for Enhanced Activity in Carbon Dioxide

Photocatalytic Reduction. ChemPhotoChem 2021;5:438–44. https://doi.org/10.1002/cptc.202000295.

[117] Che Y, Lu B, Qi Q, Chang H, Zhai J, Wang K, et al. Bio-inspired Z-scheme g-C3N4/Ag2CrO4 for efficient visible-light photocatalytic hydrogen generation. Sci Rep 2018;8:1–12. https://doi.org/10.1038/s41598-018-34287-w.

[118] Sun N, Zhou M, Ma X, Cheng Z, Wu J, Qi Y, et al. Self-assembled spherical In2O3/BiOI heterojunctions for enhanced photocatalytic CO2 reduction activity. Journal of CO2 Utilization 2022;65:102220. https://doi.org/10.1016/J.JCOU.2022.102220.

[119] Xu F, Meng K, Cheng B, Wang S, Xu J, Yu J. Unique S-scheme heterojunctions in self-assembled TiO2/CsPbBr3 hybrids for CO2 photoreduction. Nat Commun 2020;11:1–9. https://doi.org/10.1038/s41467-020-18350-7.

[120] Xu Q, Zhang L, Cheng B, Fan J, Yu J. S-Scheme Heterojunction Photocatalyst. Chem 2020;6:1543–59. https://doi.org/10.1016/j.chempr.2020.06.010.

[121] Zhang X, Kim D, Yan J, Lee LYS. Photocatalytic CO2Reduction Enabled by Interfacial S-Scheme Heterojunction between Ultrasmall Copper Phosphosulfide and g-C3N4. ACS Appl Mater Interfaces 2021;13:9762–70. https://doi.org/10.1021/acsami.0c17926.

[122] Wang L, Cheng B, Zhang L, Yu J. In situ Irradiated XPS Investigation on S-Scheme TiO2@ZnIn2S4 Photocatalyst for Efficient Photocatalytic CO2 Reduction. Small 2021;17. https://doi.org/10.1002/smll.202103447.

[123] Li D, Zhou J, Zhang Z, Jiang Y, Dong Z, Xu J, et al. Enhanced Photocatalytic Activity for CO2Reduction over a CsPbBr3/CoAl-LDH Composite: Insight into the S-Scheme Charge Transfer Mechanism. ACS Appl Energy Mater 2022. https://doi.org/10.1021/acsaem.2c00612.

[124] Wang Y, He W, Xiong J, Tang Z, Wei Y, Wang X, et al. MIL-68 (In)-derived In2O3@TiO2 S-scheme heterojunction with hierarchical hollow structure for selective photoconversion of CO2 to hydrocarbon fuels. Fuel 2023;331. https://doi.org/10.1016/j.fuel.2022.125719.

[125] Zhang L, Zhang J, Yu H, Yu J. Emerging S-Scheme Photocatalyst. Advanced Materials 2022;34. https://doi.org/10.1002/adma.202107668.

[126] Gai P, Yu W, Zhao H, Qi R, Li F, Liu L, et al. Solar-Powered Organic Semiconductor–Bacteria Biohybrids for CO2 Reduction into Acetic Acid. Angewandte Chemie - International Edition 2020;59:7224–9. https://doi.org/10.1002/anie.202001047.